Journal of Palaeogeography

ORIGINAL ARTICLE Open Access

Characteristics and evolution of inertinite abundance and atmospheric pO_2 during China's coal-forming periods

Dong-Dong Wang[1], Lu-Sheng Yin[1], Long-Yi Shao[2*], Da-Wei Lyu[1], Hai-Yan Liu[1], Shuai Wang[2] and Guo-Qi Dong[2]

Abstract

Coal, especially the inertinite in it, is highly sensitive to climate changes, showing an obvious response to paleoclimate conditions, in particular, to paleo-oxygen concentration (pO_2). In this study, the inertinite abundance data of typical coal-forming periods in China were systematically collected and analyzed. Its characteristics and control factors were studied, and its evolution was established. Based on inertinite abundance data, pO_2 evolution curves of various coal-forming periods in China were established, which fluctuated between 15% and 30% during the entire Phanerozoic. The inertinite abundance in coal deposits during Paleozoic in China was basically consistent with that of other areas of the world, while it was quite different globally from the Mesozoic to the Cenozoic. The results show that the inertinite abundance in coal deposits is controlled by pO_2 and other factors including climatic zones, plant differentiation, sedimentary environments, and tectonic activities. The inertinite abundance in coal deposits in China during the Jurassic was high, suggesting dry paleoclimate of inland China.

Keywords: Inertinite abundance, pO_2, Paleoclimate, Sedimentary environment, Coal-forming period, Comparative analysis, China

1 Introduction

Coal is considered to be highly sensitive to climate changes. The maceral types and composition reflect paleoclimatic conditions during coal forming periods (Stach 1990), particularly the inertinite abundance (Diessel 2010). Inertinite is formed by fusainization of coal-forming materials during peatification stage, and generally reflects relatively dry conditions (Stach 1990; Teichmüller 1989). At present, there are many disagreements on the genesis of inertinite, related to oxidation (Corrêa-da-Silva and Wolf 1980; Falcon 1989; Hunt 1989; Taylor et al. 1989; Silva and Kalkreuth 2005; Silva et al. 2008; Van Niekerk et al. 2010; Hower et al. 2011; Richardson et al. 2012; Wang et al. 2016) and fire (Bustin 1997; Scott 2000; Scott and Glasspool 2007; Diessel 2010; Hudspith et al. 2012; Shao et al. 2017). Diessel (2010) examined the overall distributions of global stratigraphy, and found that incomplete combustion was the main source of inertinite in coal. The genesis of inertinite requires a high oxygen content in atmosphere during coal-forming periods. Therefore, relatively dry oxidation conditions would be favorable for inertinite forming.

In accordance with the findings presented by Scott (2000, 2002), Scott et al. (2000), and Scott and Glasspool (2006, 2007), a correlation exists between the inertinite content in coal and the atmospheric oxygen levels at the time of formation. The forming of inertinite is affected by atmospheric paleo-oxygen concentrations (pO_2) during the coal-forming periods (Robinson 1989; Scott and Glasspool 2007; Diessel 2010; Sen et al. 2016). At a global scale, the pO_2 is considered to be the main factor controlling the inertinite abundance in coal. And local areas, paleoclimate conditions may also lead to different inertinite abundance (Diessel 2010). Therefore, based on

* Correspondence: shaol@cumtb.edu.cn
[2]College of Geoscience and Surveying Engineering, China University of Mining and Technology (Beijing), Beijing 100083, China
Full list of author information is available at the end of the article

the correlations between inertinite and pO_2, researchers have speculated that the inertinite abundance in coal since the Paleozoic can be used to quantify the pO_2 during coal-forming periods. Consequently, a quantitative calculation formula was put forward (Robinson 1991; Wildman et al. 2004; Scott and Glasspool 2007; Glasspool and Scott 2010; Glasspool et al. 2015).

At present, researches involved in characteristics and evolution of inertinite abundance and pO_2 during coal-forming periods in geological history are relatively less, and no unified understanding has been acquired globally. China, with a large area, experienced many coal-forming periods over a long span of time, and therefore, is favorable for case studies of coal formation. In this study, the inertinite abundance data in coal during each coal-forming period in China were systematically collected and analyzed. Characteristics of the inertinite were analyzed and evolution pathways were successfully determined, and the evolution curves of pO_2 were established as well. Comparative studies have been carried out around the world to further enrich basic theories. We hope that our findings would help supplement and better understand the previous research results and in the global range to a certain extent.

2 Data sources and pO_2 reconstruction method

2.1 Data sources

In this study, the inertinite abundance data during each coal-forming period were obtained from a wide range of sources and samples as follows: *Atlas for Coal Petrography of China* (Yang 1996); *Coal Petrology of China* (Han 1996); published data in available academic resources; national coal resources potential evaluation report (Sun, 2013); parts of the provincial coal resources potential evaluation reports (Sun, 2013); and parts of the internal research reports, as well as portions of our own laboratory test results.

In order to avoid any error which could be potentially caused by different test conditions and descriptions of test data from different sources, the abundance data were first uniformly sorted and classified. For example, the inertinite abundance of coal was determined as the percentage of inertinite in total organic matter of coal. It is assumed that the coal is mineral-matter free. In order to ensure wide coverage and high representativeness of the data points, within the scope of small errors, the similar data points from the same region and during the same period were combined, and their mean values were selected. The data points with large changes in value during the same period and in the same area should be fully reflected as representatives.

In addition, statistical methods were used to systematically collate the inertinite abundance data from different sources during coal-forming periods, which include: mean abundance of inertinite; sample numbers; maximum values; minimum values; and standard deviations, as well as literary sources and regional distribution of data (Tables 1, 2, 3, 4, 5 and 6). The stratigraphic divisions and chronology framework used in this study referenced the 2014 edition of the *China Stratigraphic Chart* proposed in the attached table of the All China Commission of Stratigraphy (2015).

2.2 Reconstruction method of pO_2 during coal-forming periods

There are only a few studies about calculating pO_2 from inertinite abundance in coal. In this study, the most-highly-recognized pO_2 reconstruction model and an exponential function formula (Glasspool and Scott 2010) were applied, based on the following known conditions:

1) When $pO_2 \leq 15\%$, charcoal is basically not produced (which means that the inertinite abundance is close to 0%) (Belcher and McElwain 2008). Under such conditions, in a typical coal rock, only one charcoal particle out of ≥500 counts, was found, and therefore, the inertinite abundance was considered to be 0.2% (Taylor et al. 1998).
2) The oxygen concentration in the modern atmosphere is approximately 21%. Based on a series of peat tests produced under different ecological, climatic, and geographical conditions, the inertinite abundance has been determined to be approximately 4.3% (Glasspool and Scott 2010).
3) Several studies have determined the upper limit of Phanerozoic pO_2 and its corresponding inertinite. Combustion experiments by Belcher and McElwain (2008) revealed that the upper limits of fully-burnt oxygen range between 25% and 35%. Therefore, pO_2 with a median value of 30% was taken as the upper limit of fully-burnt oxygen (Glasspool et al. 2015). Lenton and Watson (2000) determined that an inertinite abundance of 44.4% was related to a pO_2 of 30%.

Therefore, based on the above-mentioned information, this study estimated and calibrated the pO_2 based on inertinite abundance as follows: 15% pO_2 corresponds to 0.2% inertinite abundance; 21% pO_2 corresponds to 4.3% inertinite abundance; and 30% pO_2 corresponds to 44.4% inertinite abundance. Subsequently, an exponential function of pO_2 and inertinite abundance was established using data processing software, with a high correlation coefficient R^2 value ($R^2 = 0.99$). The equation is as follows (Glasspool and Scott 2010):

Table 1 The inertinite abundance and pO_2 characteristics in Middle Devonian coals in China. I_{AVG}: Mean inertinite abundance; N: Samples number; R: Percentage range; S: Standard deviation

Literature source	I_{AVG}, %	N	R (min–max), %	S	pO_2, %	Stage/Formation/Locality	Province
Dai et al. 2006	0.1	8	0–0.7	0.2	14	Dongganglingian (Givetian)/Qujing F./Luquan	Yunnan
Han 1996	0.7	2	0.5–0.8	0.2	17	Dongganglingian (Givetian)/Haikou F./Panzhihua Barley Field	Sichuan
	3.0	2	2.6–3.4	0.4	21	Dongganglingian (Givetian)/Haikou F./Panzhihua, Shaping	Sichuan

$$pO_2 = 18.113 \times \left(\text{Inertinite}\%^{0.1273}\right)$$

According to the above equation, the mean inertinite abundance during each coal-forming period could be converted into pO_2. In this way, the pO_2 evolution curve during coal-forming periods of the entire Phanerozoic Eon was successfully reconstructed. This method supplements the research of global pO_2 evolution in geological history.

3 Inertinite abundance and pO_2 characteristics during different coal-forming periods

Atmospheric pO_2 is closely related to the evolution of lignocellulosic plants (Mills et al. 2016), and plays an indispensable role in biochemical cycles of the Earth (Berner 1999). The emergence of terrestrial plants, along with the development of lignin at the end Silurian, facilitated the formation of large-scale peat and coal deposits (Wang 2002). Subsequently, inertinite-containing strata began to appear and continued to the present day (Premovic 2006). Therefore, the long-term changes in atmospheric pO_2 in geological history may potentially explain the distribution and abundance of inertinite in coal deposits (Diessel 2010).

Statistical tables of inertinite abundance and pO_2 during different coal-forming periods in China were completed in Tables 1, 2, 3, 4, 5 and 6, and the spatial distributions of related data points were plotted in Fig. 1.

3.1 Devonian

During the Devonian, plants evolved systematically, and a large number of aquatic plants moved towards land. The diversity of plant systems, and their amazing abilities to reproduce and grow, laid the foundation for the formation of higher plants on land. It has been discovered that during the Late Silurian (Rimmer and Scott 2006) and Early Devonian (Glasspool et al. 2006), an inertinite in the form of charcoal appeared for the first time in the world.

The Devonian is considered to be one of the most important coal-forming periods in China, during which both southern and northern China were characterized by tropical climate conditions (Li and Jiang 2013). The Early Devonian plants were in the early stages of growth and were considered to be higher terrestrial plants. They grew in clusters around coastal wetland areas with limited coverage, and generally formed thin coal seams. During the Middle Devonian, sea level fluctuated frequently, and plants were further propagated in low-lying areas, such as coastal boughs and lagoons. Coal seams were also formed in those areas (Han et al. 1993). Tectonic movements and transgression in southern China had profound influence on the development of coal basins and the formation of coal deposits (Zhang 1995; Li et al. 2018). It has been determined that during the Devonian, coal-bearing strata in China were mainly distributed in the southwestern regions, which mainly developed during the Dongganglingian (Givetian) of Middle Devonian, such as the Haikou Formation in Panzhihua of Sichuan Province, and the Qujing Formation in Luquan of Yunnan Province.

Devonian coal seams are generally thin, ranging between 0.1 m and 0.3 m, characterized by the low abundance and limited distribution of inertinite. The majority inertinite abundance ranges between 0.1% and 3.0% (Table 1). Correspondingly, the overall pO_2 was not high. It was approximately 15% during Early Devonian, and increased significantly during Middle and Late Devonian, and reached approximately 20% by Late Devonian.

3.2 Carboniferous–Permian

During the Carboniferous–Permian period, the southern and northern China were under tropical climate conditions (Tabor and Poulsen 2008) with significantly-increased diversity of terrestrial plants (mainly ferns and gymnosperms), leading to profound changes in inertinite type and abundance (Table 2).

3.2.1 Early carboniferous

During Early Carboniferous, coal-bearing strata were widely distributed in the southern China. Under humid and rainy tropical climates, plants as Calamites and Sublepidodendron formed dense forests (Yang 1996), which mainly distributed in coastal lowlands, and did not show obvious climatic differentiation and palaeogeographical isolation (Liu and Quan 1996). The preservation condition for lignin in the plants had been continuously improved, which was conducive to the formation and preservation of coal seams (Diessel 2010). In southern China, the coal seams were mainly developed in deltaic environments, followed by meandering river–lake

Table 2 The inertinite abundance and pO_2 characteristics in Carboniferous–Permian coals in China. I_{AVG}: Mean inertinite abundance; N: Samples number; R: Percentage range; S: Standard deviation

Literature source	I_{AVG}, %	N	R (min–max), %	S	pO_2, %	Stage/Formation/Locality	Province
Early Carboniferous							
Han 1996	12.2	3	6.1–21.2	6.5	25	Visean/Chouniugou F./Jingyuan	Gansu
Potential evaluation of coal resources in Yunnan	11.0	2	10.8–11.2	0.2	25	Visean/Wanshoushan F./Dianzhong	Yunnan
Potential evaluation of coal resources in Guangxi	14.0	2	13.0–15.0	1.0	25	Dewuan (Serpukhovian)/Simen F./Datang	Guangxi
Yang 1996	10.7	4	5.0–22.3	7.0	24	Dewuan (Serpukhovian)/Ceshui F./Huaihua	Hunan
	20.2	1			27	Dewuan (Serpukhovian)/Ceshui F./Shuangfeng	Hunan
	14.5	1			25	Dewuan (Serpukhovian)/Ceshui F./Xinhua	Hunan
	5.6	1			23	Dewuan (Serpukhovian)/Ceshui F./Huishanxiang	Hunan
Late Carboniferous–Early Permian							
Han 1996	23.6	1			27	Xiaoyiaoan (Kasimovian–Gzhelian)/Taiyuan F./Shizuishan	Ningxia
	19.1	2	18.5–19.6	0.6	26	Xiaoyiaoan (Kasimovian–Gzhelian)/Taiyuan F./Wuda	Inner Mongolia
	28.0	10	1.7–59.3	15.2	28	Xiaoyiaoan (Kasimovian–Gzhelian)/Taiyuan F./Datong	Shanxi
	28.6	7	20.9–50.0	9.8	28	Xiaoyiaoan (Kasimovian–Gzhelian)/Taiyuan F./Tangshan	Hebei
	23.6	1			27	Xiaoyiaoan (Kasimovian–Gzhelian)/Taiyuan F./Nanpiao	Liaoning
	25.2	5	10.6–47.0	12.1	27	Xiaoyiaoan (Kasimovian–Gzhelian)/Taiyuan F./Tongchuan	Shaanxi
	9.7	2	7.4–12.0	2.3	24	Xiaoyiaoan (Kasimovian–Gzhelian)/Taiyuan F./Pingdingshan	Henan
	12.4	6	7.0–18.0	4.0	25	Xiaoyiaoan (Kasimovian–Gzhelian)/Taiyuan F./Luzhong	Shandong
	8.3	2	6.5–10.0	1.8	24	Xiaoyiaoan (Kasimovian–Gzhelian)/Taiyuan F./Xuzhou	Jiangsu
Dai et al. 2006	37.4	7			29	Xiaoyiaoan (Kasimovian–Gzhelian)/Taiyuan F./Ordos Basin	Inner Mongolia
Dai et al. 2008	58.8	1			30	Xiaoyiaoan (Kasimovian–Gzhelian)/Taiyuan F./Junggar Coalfield	Inner Mongolia
Xiao et al. 2005	32.5	13		5.2	28	Xiaoyiaoan (Kasimovian–Gzhelian)/Taiyuan F./Ordos Basin	Gansu, Shaanxi, and Inner Mongolia
Querol et al. 1999	10.3	4		4.9	24	Xiaoyiaoan (Kasimovian–Gzhelian)/Taiyuan F./Luxi area	Shandong
Liu et al. 2004	12.9	6		3.9	25	Xiaoyiaoan (Kasimovian–Gzhelian)/Taiyuan F./Yanzhou	Shandong
Zhou et al. 1990	17.1	22		5.9	26	Xiaoyiaoan (Kasimovian–Gzhelian)/Taiyuan F./Pingdingshan	Henan
Sun et al. 2002	3.0	1			21	Xiaoyiaoan (Kasimovian–Gzhelian)/Shanxi F./Xingtai	Hebei
Querol et al. 1999	20.5	3		2.4	27	Zisongian (Asselian–Sakmarian)/Shanxi F./Luxi area	Shandong
Sun et al. 2002	45.0	11		8.7	29	Zisongian (Asselian–Sakmarian)/Shanxi F./Xingtai	Hebei
Li et al. 1997	37.4	45			29	Zisongian (Asselian–Sakmarian)/Shanxi F./Huabei Basin	Henan Shanxi
Xiao et al. 2005	35.1	32		7.5	28	Zisongian (Asselian–Sakmarian)/Shanxi F./Ordos Basin	Inner Mongolia
Han 1996	9.2	5	3.5–12.4	3.1	24	Zisongian (Asselian–Sakmarian)/Chuanshan F./Longyan	Fujian

Table 2 The inertinite abundance and pO_2 characteristics in Carboniferous–Permian coals in China. I_{AVG}: Mean inertinite abundance; N: Samples number; R: Percentage range; S: Standard deviation *(Continued)*

Literature source	I_{AVG}, %	N	R (min–max), %	S	pO_2, %	Stage/Formation/Locality	Province
Li et al. 1997	20.0	28			27	Zisongian (Asselian–Sakmarian)/Taiyuan F./Huabei Basin	Henan Shanxi
Potential evaluation of coal resources in Inner Mongolia	18.4	1			26	Longlinian (Artinskian)/Taiyuan F./Zhuozishan Mining area	Inner Mongolia
Yang 1996	51.6	2	45.3–57.9	6.3	30	Longlinian (Artinskian)/Taiyuan F./Junggar Basin	Inner Mongolia
	42.6	2	34.6–50.6	8.0	29	Longlinian (Artinskian)/Taiyuan F./Shizuishan	Ningxia
	34.3	6	23.7–55.6	11.5	28	Longlinian (Artinskian)/Taiyuan F./Datong	Shanxi
	24.9	2	13.4–36.4	11.5	27	Longlinian (Artinskian)/Taiyuan F./Fengfeng	Hebei
	11.1	5	8.6–15.7	2.6	25	Longlinian (Artinskian)/Taiyuan F./Luxinan area	Shandong
	8.5	3	7.5–10.5	1.4	24	Longlinian (Artinskian)/Taiyuan F./Xuzhou	Jiangsu
	39.1	3	35.9–41.9	2.5	29	Longlinian (L. Artinskian)/Shanxi F./Wuhai	Inner Mongolia
	37.9	2	28.0–47.8	9.9	29	Longlinian (L. Artinskian)/Shanxi F./Shizuishan	Ningxia
	15.9	3	8.8–19.7	5.0	26	Longlinian (L. Artinskian)/Shanxi F./Wubao	Shaanxi
	32.9	6	19.4–45.3	9.1	28	Longlinian (L. Artinskian)/Shanxi F./Jinbei area	Shanxi
	32.9	6	27.6–35.7	2.5	28	Longlinian (L. Artinskian)/Shanxi F./Jixi area	Hebei
	27.9	8	18.0–40.0	6.9	28	Longlinian (L. Artinskian)/Shanxi F./Luxi area	Shandong
	24.3	2	24.1–24.5	0.2	27	Longlinian (L. Artinskian)/Shanxi F./Lianghuai/	Anhui
	33.3	3	30.0–37.0	2.9	28	Longlinian (L. Artinskian)/Shanxi F./Xuzhou	Jiangsu
	26.0	1			27	Longlinian (L. Artinskian)/Shanxi F./Pingdingshan	Liaoning
	18.5	7	6.2–29.1	8.0	26	Longlinian (L. Artinskian)/Shanxi F./Wanbei area	Henan
	10.0	2	5.6–14.3	4.4	24	Luodianian (E. Kungurian)/Liangshan F./Huaihua	Hunan
	6.4	7	2.0–16.0	4.8	23	Luodianian (E. Kungurian)/Liangshan F./Tongshan	Hubei
Mu-Qiu 1979	20.6	18		20.3	27	Luodianian (Kungurian)/Shanxi F./Kailuan Basin	Hebei
Middle Permian							
Yang 1996	13.8	1			25	Luodianian–Xiangboan (Kungurian)/Liangshan F./Chenxi	Hunan
	15.0	1			26	Luodianian–Xiangboan (Kungurian)/Liangshan F./Chenxi	Hubei
	58.3	4	35.0–78.0	15.7	30	Luodianian–Xiangboan (Kungurian)/Liangshan F./Yuebei area	Guangdong
	20.0	1			27	Luodianian–Xiangboan (Kungurian)/Liangshan F./Dianbei area	Yunnan
	21.0	5	14.7–34.6	7.2	27	Xiangboan (L. Kungurian–E. Roadian)/L. Shihezi F./Huainan	Anhui
	45.3	2	35.8–54.8	9.5	29	Xiangboan (L. Kungurian–E. Roadian)/L. Shihezi F./Suzhou	Anhui
	22.6	1			27	Xiangboan (L. Kungurian–E. Roadian)/L. Shihezi F./Huaibei	Anhui
	29.5	1			28	Xiangboan (L. Kungurian–E. Roadian)/L. Shihezi F./Xuzhou	Jiangsu
	33.6	1			28	Xiangboan (L. Kungurian–E. Roadian)/L. Shihezi F./Pingdingshan	Henan

Table 2 The inertinite abundance and pO_2 characteristics in Carboniferous–Permian coals in China. I_{AVG}: Mean inertinite abundance; N: Samples number; R: Percentage range; S: Standard deviation *(Continued)*

Literature source	I_{AVG}, %	N	R (min–max), %	S	pO_2, %	Stage/Formation/Locality	Province
Han 1996	7.9	2	5.7–10.0	2.2	24	Xiangboan (L. Kungurian–E. Roadian)/L. Shihezi F./Suzhou	Anhui
	6.5	10	2.7–9.6	1.9	23	Lengwuan (Capitanian)/Tongziyan F./Yongding	Fujian
Yang 1996	42.1	2	40.5–43.6	1.6	29	Lengwuan (Capitanian)/U. Shihezi F./Huaibei	Anhui
	23.0	4	15.8–30.5	5.5	27	Lengwuan (Capitanian)/U. Shihezi F./Huainan	Anhui
	28.5	2	15.0–42.0	13.5	28	Lengwuan (Capitanian)/Tongziyan F./Meizhou	Guangdong
Late Permian							
Yang 1996	9.4	6	5.6–11.2	2.0	24	Wuchiapingian/Longtan F./Edong	Hubei
	18.1	5	9.8–30.0	7.7	26	Wuchiapingian/Longtan F./Shaoguan	Guangdong
	21.1	5	14.0–32.6	6.7	27	Wuchiapingian/Longtan F./Qujing	Yunnan
	10.1	5	2.8–22.0	6.7	24	Wuchiapingian/Longtan F./Guizhong area	Guangxi
	13.0	2	7.0–19.0	6.0	25	Wuchiapingian/Longtan F./Guangde	Anhui
	15.6	1			26	Wuchiapingian/Longtan F./Changxing	Zhejiang
	20.5	3	14.2–31.4	7.7	27	Wuchiapingian/Longtan F./Sunan area	Jiangsu
	20.7	4	8.6–36.8	10.6	27	Wuchiapingian/Longtan F./Jiujiang	Jiangxi
Querol et al. 2001	20.3	8	2.2–26.8	12.9	27	Wuchiapingian/Longtan F./Leping	Jiangxi
Shao et al. 2003	21.8	5		5.4	27	Wuchiapingian/Longtan F./Heshan	Guangxi
Dai et al. 2005	15.7	2			26	Wuchiapingian/Longtan F./Dafang	Guizhou
Zhuang et al. 2007	11.8	9		2.5	25	Wuchiapingian/Longtan F./Chahe	Guizhou
Wollenweber et al. 2006	16.5	1			26	Wuchiapingian/Longtan F./South China Dahe Coal Mine	Guizhou
Querol et al. 2001	31.2	1			28	Changhsingian/Changxing F./Leping	Jiangxi
Yang 1996	33.3	2	29.0–37.5	4.3	28	Changhsingian/Changxing F./Anxian	Sichuan
	2.4	1			20	Changhsingian/Changxing F./Tianfu	Sichuan
	6.1	4	4.3–8.7	1.6	23	Changhsingian/Changxing F./Nantong	Chongqing
	13.4	7	9.7–16.1	2.0	25	Changhsingian/Changxing F./Qianxibei area	Guizhou
Han 1996	20.6	4	19.3–23.2	1.6	27	Changhsingian/Changxing F./Xiangxi area	Hunan
	29.3	6	23.7–42.4	6.4	28	Changhsingian/Wangjiazhai F./Liupanshui	Guizhou
	30.7	1			28	Changhsingian/Wangjiazhai F./Qiannan	Guizhou
Dai et al. 2003	25.6	5		9.6	27	Changhsingian/Wangjiazhai F./Zhijin	Guizhou

Table 3 The inertinite abundance and pO_2 characteristics in Late Triassic coal-bearing strata in China. I_{AVG}: Mean inertinite abundance; N: Samples number; R: Percentage range; S: Standard deviation

Literature source	I_{AVG}, %	N	R (min–max), %	S	pO_2, %	Stage/Formation/Locality	Province
Late Triassic							
Han 1996	19.5	3	15.6–26.1	4.7	26	Yazhiliangian (Carnian)/Maantang F./Zixing	Hunan
	7.9	1			24	Yazhiliangian (Carnian)/Maantang F./Yangmeishan	Hunan
	8.6	5	1.7–15.2	4.4	24	Yazhiliangian (Carnian)/Zijiachong F./Xiangdong area	Hunan
Yang 1996	28.4	9	16.8–37.8	6.7	28	Peikucuo Stage (Norian)/Daqiaodi F./Southwestern Sichuan	Sichuan
	23.2	4	13.1–36.8	9.3	27	Peikucuo Stage (Norian)/Xiaotangzi F./Tiefo	Sichuan
Han 1996	20.1	2	1.8–38.3	18.3	27	Peikucuo Stage (Norian)/Xiaotangzi F./Xiangyun	Yunnan
	14.4	4	10.1–19.5	3.9	25	Peikucuo Stage (Rhaetian)/Xujiahe F.	Sichuan
	26.3	4	10.8–35.3	9.7	27	Peikucuo Stage (Rhaetian)/Xujiahe F./Guangyuan	Sichuan
Yang 1996	7.4	2	7.2–7.6	0.2	23	Peikucuo Stage (Rhaetian)/Xujiahe F./Yipinglang	Yunnan
	24.0	1			27	Peikucuo Stage (Rhaetian)/Xujiahe F./Suijiang	Yunnan
	6.5	1			23	Peikucuo Stage (Rhaetian)/Xujiahe F./Zigui	Hubei
	5.8	2	5.4–6.2	0.4	23	Peikucuo Stage (Rhaetian)/Xujiahe F./Nanling	Guangdong
	16.8	1			26	Peikucuo Stage (Rhaetian)/Xujiahe F./Xingren	Guizhou
Zhuang et al. 2007	18.4	3		2.0	26	Peikucuo Stage (Rhaetian)/Xujiahe F.	Chongqing/Hubei
Querol et al. 2001	1.1	2	0.2–1.9		18	Peikucuo Stage (L. Triassic)/Anyuan F./Leping	Jiangxi
Han 1996	14.5	3	10.3–21.2	4.8	25	Peikucuo Stage (L. Triassic)/Anyuan F./Pingxiang	Jiangxi
	21.2	1			27	Peikucuo Stage (L. Triassic)/Anyuan F./Pingxiang	Jiangxi
	24.8	1			27	Peikucuo Stage (Rhaetian)/Wayaobao F./Ordos Basin	Shaanxi

environments, alluvial fan–braided river environments, and tidal flat–coastal environments, respectively (Liu 1990; Zhang 1995; Zheng 2008).

The coal-bearing strata of the Early Carboniferous were mainly distributed in the Ceshui Formation of Dewuan (Serpukhovian) Stage in central Hunan Province; Simen Formation of Visean Stage in Guangxi Province; and Wanshoushan Formation of Visean Stage in Yunnan Province. In addition, it has also been determined that in northwestern China, such locations as Chouniugou Formation of Visean Stage in Jingyuan, Gansu were also conducive to coal deposits.

The mean inertinite abundance in coals of the southern China during Early Carboniferous ranged between 5.6% and 20.2%, with the largest variation (5.0%–22.3%) observed in Ceshui Formation in different areas of Hunan Province. In Datang area of Guangxi, the value ranged between 13.0% and 15.0%, with an average of 14.0%. The pO_2 during Early Carboniferous had increased compared to that of Devonian, and remained stable around 25%.

3.2.2 Late Carboniferous–Early Permian

From Late Carboniferous to Early Permian, coal-bearing strata mainly developed in the basins of North China, with humid climate conditions (Chang and Gao 1993; Tan 2017), and extended stable tectonic setting. Coal-forming processes were active in the following formations: Taiyuan Formation of Xiaoyiaoan–Longlinian (Kasimovian–Artinskian) Stages; Shanxi Formation of Zisongian–Longlinian (Asselian–Artinskian) Stages; and Liangshan Formation of Luodianian–Xiangboan (Kungurian–early Roadian) Stages (which spanned the Lower and Middle Permian). (1) In Taiyuan Formation of Xiaoyiaoan Stage (Kasimovian–Gzhelian), the mean inertinite abundance in coals ranges between 19.1% and 58.8%, with relatively high values occurring in the Ordos Basin. In the area of Jiangsu–Shandong–Henan, this value ranges between 8.3% and 28.6%. (2) In Taiyuan Formation of Zisongian–Longlinian (Asselian–Artinskian) Stages, the mean inertinite abundance remains high with significant variations, with the highest value of 51.6% occurring in Junggar Basin, and the lowest of 8.5% occurring in northern Jiangsu Province. (3) In Shanxi Formation of Zisongian–Longlinian (Asselian–Artinskian) Stages, the inertinite abundance slightly decreased when compared to the values of previous periods, ranging between 15.9% and 45.0%, (4) The inertinite abundance decreased from west to east from Taiyuan Formation to Shanxi Formation (Han 1996). (5) In the Liangshan

Table 4 The inertinite abundance and pO_2 characteristics in Early–Middle Jurassic coal-bearing strata in China. I_{AVG}: Mean inertinite abundance; N: Samples number; R: Percentage range; S: Standard deviation

Literature source	I_{AVG}, %	N	R (min–max), %	S	pO_2, %	Stage/Formation/Locality	Province
Early Jurassic							
Yang 1996	3.5	2	2.8–4.2	0.7	21	Yongfeng Stage (Hettangian–Sinemurian)/Badaowan F./Karamay	Xinjiang
	9.5	2	8.0–11.0	1.5	24	Yongfeng Stage (Hettangian–Sinemurian)/Badaowan F./Wusu	Xinjiang
	14.8	5	11.0–18.4	2.4	26	Yongfeng Stage (Hettangian–Sinemurian)/Badaowan F./Changji	Xinjiang
	3.3	3	2.6–4.8	1.0	21	Yongfeng Stage (Hettangian–Sinemurian)/Badaowan F./Baicheng	Xinjiang
	39.5	3	38.0–40.5	1.1	29	Liuhuanggou Stage (Pliensbachian–Toarcian)/Xishanyao F./Hami Basin	Xinjiang
	4.7	2	4.3–5.0	0.4	26	Liuhuanggou Stage (Pliensbachian–Toarcian)/Xishanyao F./Hami Basin	Xinjiang
	36.5	3	24.3–43.1	8.7	29	Liuhuanggou Stage (Pliensbachian–Toarcian)/Xishanyao F./Yili Basin	Xinjiang
	49.0	3	40.7–61.5	9.0	30	Liuhuanggou Stage (Pliensbachian–Toarcian)/Xishanyao F./Yili Basin	Xinjiang
	18.3	3	13.6–21.8	3.5	26	Liuhuanggou Stage (Pliensbachian–Toarcian)/Xishanyao F./Baicheng	Xinjiang
	34.1	4	23.3–44.5	9.8	28	Liuhuanggou Stage (Pliensbachian–Toarcian)/Xishanyao F./Tarim Basin	Xinjiang
	20.4	1			27	Shihezi Stage (Aalenian–Bajocian)/Xiahuayuan F./Fangzi	Shandong
Potential evaluation of coal resources in Hebei	39.1	5	11.3–71.9	21.4	29	Shihezi Stage (Aalenian–Bajocian)/Xiahuayuan F./Xuanhua	Hebei
Middle Jurassic							
Yang 1996	19.7	3	15.0–24.0	3.7	26	Shihezi Stage (Aalenian–Bajocian)/Xintiangou F./Xiwan	Guangxi
	19.0	1			26	Shihezi Stage (Aalenian–Bajocian)/Xintiangou F./Hualong	Zhejiang
	35.0	2	10.0–59.9	25.0	28	Shihezi Stage (Aalenian–Bajocian)/Xintiangou F./Guangwang	Sichuan
	71.5	2	69.1–81.5	7.3	31	Shihezi Stage (Aalenian–Bajocian)/Yan'an F./Dongsheng (Ordos Basin)	Inner Mongolia
	31.9	2	28.4–35.4	3.5	28	Shihezi Stage (Aalenian–Bajocian)/Yan'an F./Dongsheng (Ordos Basin)	Inner Mongolia
	50.3	4	48.1–54.3	2.5	30	Shihezi Stage (Aalenian–Bajocian)/Yan'an F./Ordos Basin	Shaanxi
	57.6	4	38.6–73.8	14.5	30	Shihezi Stage (Aalenian–Bajocian)/Yan'an F./Lingyan area	Ningxia
	56.3	4	46.7–69.8	9.3	30	Shihezi Stage (Aalenian–Bajocian)/Yan'an F./Huanglong Coalfield	Gansu
	45.2	4	38.3–57.1	7.3	29	Shihezi Stage (Aalenian–Bajocian)/Yan'an F./Longdong Coalfield	Gansu
	84.0	3	80.3–86.9	2.8	32	Shihezi Stage (Aalenian–Bajocian)/Yan'an F./Longdong Coalfield	Gansu
	48.0	1			30	Shihezi Stage (Aalenian–Bajocian)/Yan'an F./Longdong Coalfield	Gansu
	37.3	4	27.7–49.9	8.0	29	Shihezi Stage (Aalenian–Bajocian)/Datong F./Datong Basin	Shanxi
	26.6	2	22.3–30.8	4.3	28	Shihezi Stage (Aalenian–Bajocian)/Yima F./Yima Basin	Henan
	12.2	2	10.8–13.5	1.4	25	Shihezi Stage (Aalenian–Bajocian)/Xishanyao F./Junggar Basin	Xinjiang
	29.8	4	24.6–36.6	4.3	28	Shihezi Stage (Aalenian–Bajocian)/Xishanyao F./Junggar Basin	Xinjiang
	44.0	4	40.8–45.5	1.9	29	Shihezi Stage (Aalenian–Bajocian)/Xishanyao F./Tuha Basin	Xinjiang

Table 4 The inertinite abundance and pO_2 characteristics in Early–Middle Jurassic coal-bearing strata in China. I_{AVG}: Mean inertinite abundance; N: Samples number; R: Percentage range; S: Standard deviation *(Continued)*

Literature source	I_{AVG}, %	N	R (min–max), %	S	pO_2, %	Stage/Formation/Locality	Province
	50.7	3	47.0–55.1	3.3	30	Shihezi Stage (Aalenian–Bajocian)/Xishanyao F./Yili Basin	Xinjiang
	68.1	3	57.2–77.8	8.4	31	Shihezi Stage (Aalenian–Bajocian)/Xishanyao F./Tarim Basin	Xinjiang
	1.7	3	1.1–2.4	0.5	19	Shihezi Stage (Aalenian–Bajocian)/Yaojie F./Wuwei-Tianzhu Basin	Gansu
	45.9	6	19.4–59.6	13.1	29	Manasi Stage (Bathonian–Callovian)/Toutunhe F./Minhe Basin	Qinghai
	66.5	1			31	Manasi Stage (Bathonian–Callovian)/Toutunhe F./Minhe Basin	Qinghai
	33.1	2	29.3–36.8	3.8	28	Manasi Stage (Bathonian–Callovian)/Toutunhe F./Minhe Basin	Qinghai
	24.0	2	23.2–24.7	0.8	27	Manasi Stage (Bathonian–Callovian)/Toutunhe F./Minhe Basin	Qinghai

Table 5 The inertinite abundance and pO_2 characteristics in Early Cretaceous coal-bearing strata in China. I_{AVG}: Mean inertinite abundance; N: Samples number; R: Percentage range; S: Standard deviation

Literature source	I_{AVG}, %	N	R (min–max), %	S	pO_2, %	Stage/Formation/Locality	Province
Early Cretaceous							
Yang 1996	10.8	4	5.0–19.1	5.3	25	Jibei Stage (Berriasian–Hauterivian)/Huolinhe F./Huolinhe Coalfield	Inner Mongolia
	5.3	4	2.0–8.5	2.5	22	Jibei Stage (Berriasian–Hauterivian)/Huolinhe F./Yuanbaoshan Coalfield	Inner Mongolia
Potential evaluation of coal resources in Inner Mongolia	34.7	2	26.7–42.6	8.0	28	Jibei Stage (Berriasian–Hauterivian)/Huolinhe F./Erenhot Basin	Inner Mongolia
Han 1996	42.4	4	26.1–55.8	11.2	29	Rehei Stage (Barremian)/Yimin F./Jalainur Coalfield	Inner Mongolia
Yang 1996	37.5	2	35.0–40.0	2.5	29	Rehei Stage (Barremian)/Yimin F./Yimin Coalfield	Inner Mongolia
	25.0	2	20.0–30.0	5.0	27	Rehei Stage (Barremian)/Yixian F./Hegang Coalfield	Heilongjiang
Han 1996	9.4	11	1.2–20.8	6.1	24	Rehei Stage (Barremian)/Yixian F./Jixi Coalfield	Heilongjiang
	18.5	6	7.8–39.8	11.4	26	Rehei Stage (lower Aptian)/Jiufotang F./Boli Coalfield	Heilongjiang
	10.7	3	6.9–14.3	3.0	24	Rehei Stage (lower Aptian)/Jiufotang F./Shuangyashan Coalfield	Heilongjiang
Yang 1996	16.5	4	12.0–19.0	2.7	26	Liaoxi Stage (upper Aptian)/Shahai F./Fuxin Coalfield	Liaoning
	5.0	4	2.0–8.0	2.2	22	Liaoxi Stage (upper Aptian)/Shahai F./Tiefa Coalfield	Liaoning
	2.2	4	1.0–3.4	0.9	20	Liaoxi Stage (upper Aptian)/Shahai F./Yingcheng Coalfield	Liaoning
Potential evaluation of coal resources in Hebei	31.1	3	20.7–39.4	7.8	28	Liaoxi Stage (Aptian)/Fuxin F./Yushugou Mine Field, Guyuan	Hebei
	28.3	6	10.0–50.0	13.6	28	Liaoxi Stage (Aptian)/Fuxin F./Wanquan Coalfield	Hebei

Table 6 The inertinite abundance and pO_2 characteristics in Paleogene–Neogene coal-bearing strata in China. I_{AVG}: Mean inertinite abundance; N: Samples number; R: Percentage range; S: Standard deviation

Literature source	I_{AVG}, %	N	R (min–max), %	S	pO_2, %	Stage/Formation/Locality	Province
Paleogene							
Han 1996	1.1	5	0.8–1.5	0.3	18	Ashantou Stage (Ypresian–Lutetian)/Hunchun F./Hunchun Coalfield	Ji Lin
	1.5	4	0.4–2.2	0.7	19	Ashantou Stage (Ypresian–Lutetian)/Shulan F./Shulan Coalfield	Ji Lin
	4.5	5	0.6–7.6	3.2	22	Ashantou Stage (Ypresian–Lutetian)/Shulan F./Shulan Coalfield	Heilongjiang
	11.4	6	3.4–21.9	6.3	25	Yuanquan (Bartonian)/Lijiaya F./Liangjia Coal Mine	Shandong
According to the internal research report of Research Institute of CNOOC							
Yang 1996	4.3	3	2.3–6.0	1.5	22	Yuanquan/Lijiaya F./Yantai	Shandong
	4.6	1			22	Yuanquan/Nadu F./Baise Basin	Guangxi
	1.1	4	0.3–1.9	0.6	18	Caijiachongian (Priabonian)/Pinghu F./Xihu Depression,	East China Sea
According to the internal research report of Research Institute of CNOOC							
Zhang et al. 2010	2.6	6	1.8–3.5	0.6	20	Tabenbuluckian (Chattian)/Yacheng F./Qiongdongnan Basin	South China Sea
Potential evaluation of coal resources in Inner Mongolia	30.4	4	23.8–38.7	5.4	28	Wulanbulagean (Rupelian)/Huerjing F./Erenhot Basin	Inner Mongolia
Neogene							
Yang 1996	10.2	1			24	Shanwangian (Burdigalian)/Nanzhuang F./Nanzhuang	Taiwan
	2.6	6	1.0–5.2	1.4	20	Shanwangian/Nanzhuang F./Taipei	Taiwan
	4.1	3	0.6–6.0	2.5	22	Tonggurian (Langhian–Serravallian)/Xiaolongtan F./Xunxun	Yunnan
	4.2	3	1.3–6.5	2.2	22	Tonggurian/Tongguer F./Heze	Shandong
	3.2	7	1.5–7.3	2.0	21	Gaozhuangian (Zanclean)/Gaozhuang F./Qujing	Yunnan
	0.2	3	0.1–0.3	0.1	15	Mazegouan (Piacenzian)/Shagou F./Dianzhong	Yunnan
	4.9	3	3.4–5.8	1.1	22	Mazegouan/Shagou F./Jinsuo	Yunnan
	2.7	10	0.2–8.1	2.1	21	Mazegouan/Shagou F./Dianzhong and Baise	Yunnan /Guangxi
Qi et al. 1994	1.8	1			21	Mazegouan/Shagou F./Xunxun	Yunnan
Quaternary							
Jin and Qin 1989	4.0	1			22	Nihewanian (Gelasian–Calabrian)/Yuanma F./Tengchong	Yunnan

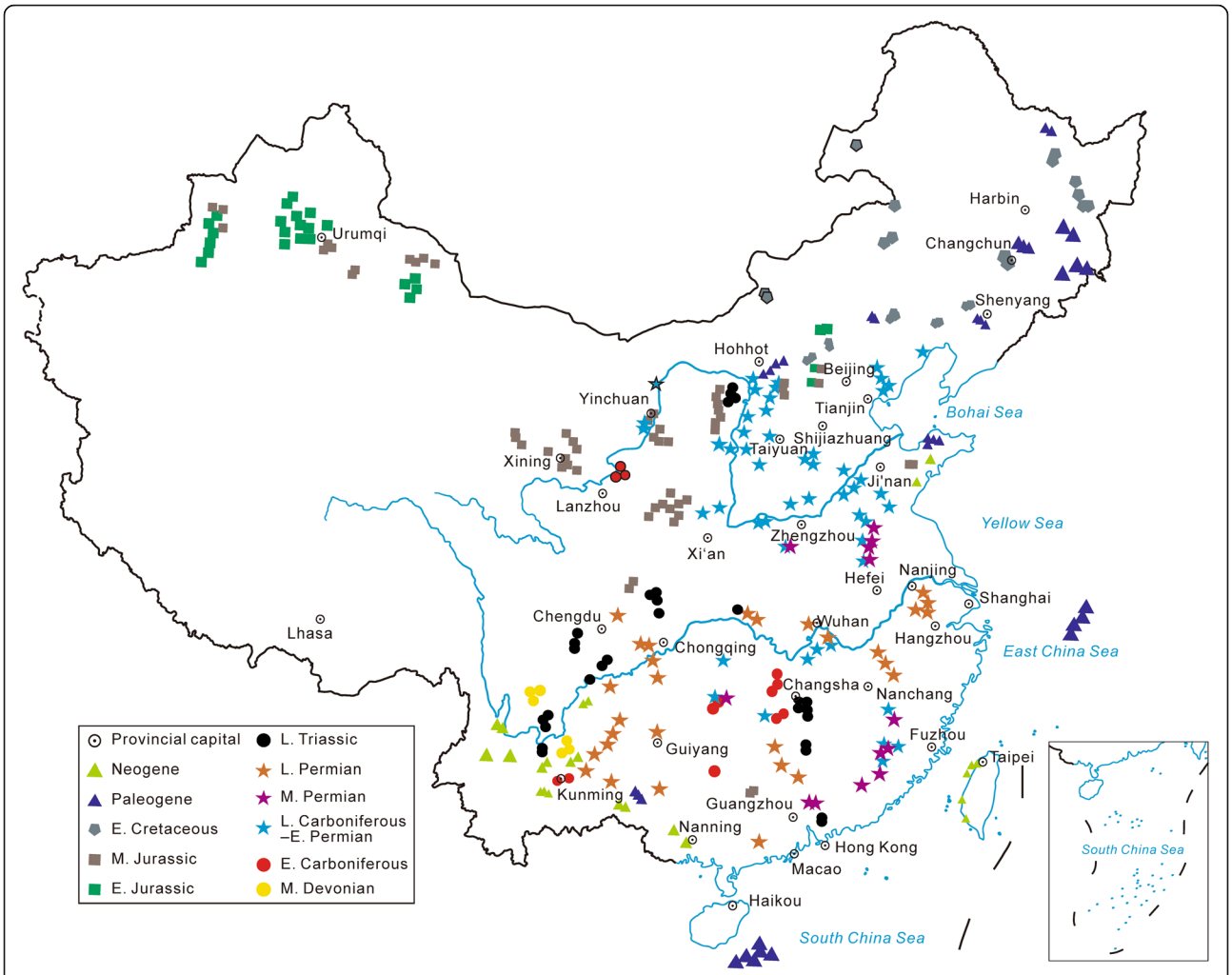

Fig. 1 Spatial distribution of the data points of inertinite abundance in coal deposits during different coal-forming periods in China. The map of China is modified after the Standard Map Service of the National Administration of Surveying, Mapping and Geoinformation of China (http://bzdt.ch.mnr.gov.cn/) (No. GS(2016)1569). E.: Early; M.: Middle; L.: Late; and the same follows

Formation of Luodianian Stage (early Kungurian), the inertinite abundance was relatively low, ranging between 6.4% and 10.0%.

During Late Carboniferous–Early Permian, the pO_2 increased significantly compared with the Early Carboniferous data. In Late Carboniferous, it reached the maximum value of almost 30%. It was above 27% throughout the Early Permian with no significant decrease and began to decrease since the late Early Permian, dropping down to approximately 24%.

3.2.3 Middle Permian

During the Middle Permian, coal-bearing strata of China were mainly developed in large-scale delta environments (Li et al. 2018), including the southern regions of northern China, west of Henan Province, southern and northern Anhui Province, Xuzhou area of Jiangsu Province, with semi-humid climate (Chang and Gao 1993; Tan 2017). Coal was mainly distributed in the following formations of Middle Permian: (1) Lower Shihezi Formation of Xiangboan Stage (late Kungurian–early Roadian), with mean inertinite abundance ranging between 7.9% and 45.3%; (2) Upper Shihezi Formation of Lengwuan Stage (Capitanian), with mean inertinite abundance ranging between 23.0% and 42.1%, and the inertinite mainly comprised of macrinite; (3) Tongziyan Formation of Lengwuan Stage (Capitanian), which was mainly distributed in Guangdong and Fujian provinces. The mean inertinite abundance varied greatly in different regions, ranging from 6.5% to 28.5%; (4) Liangshan Formation of Luodianian–Xiangboan Stages (Kungurian), of which the coal-bearing strata mainly developed during Early–Middle Permian. Coal seams were thickest in the Middle Permian, with the mean inertinite abundance ranging from 13.8% to 58.3%.

During the early Middle Permian, the pO_2 increased slightly, and remained at approximately 28% until the late Middle Permian.

3.2.4 Late Permian

During the Late Permian, coal-bearing strata in China were mainly distributed in the southern regions (Liu 1990; Zhang 1995), dominated by a semiarid climate at the early stage, and an arid climate at the late stage (Chang and Gao 1993; Tan 2017). It was also formed in an epicontinental marine environment with humid climate conditions in the early Late Permian (Golonka 2011). The distribution of coal-bearing strata was directly controlled by palaeogeographical environment, with the transgression and regression causing continuous migration of coal-rich belts (Li et al. 2018).

Coal-bearing strata were mainly developed in Longtan Formation of Wuchiapingian Stage, and in Changxing and Wangjiazhai formations of the Changhsingian Stage. (1) In Longtan Formation, the mean inertinite abundance varied among different regions: 20.3%–20.7% in eastern Jiangxi; 13.0%–15.6% in southern Anhui, southern Jiangsu and Zhejiang; and 11.8%–21.1% in Yunnan, Guizhou, and Sichuan. (2) In Changxing Formation, the value was 2.4%–33.3% in Sichuan and Chongqing with large variations. (3) In Wangjiazhai Formation, the value was 23.7%–42.4% in Guizhou, with an average of 29.3%.

During the early Late Permian, pO_2 did not vary much compared to the Middle Permian data, and remained stable at approximately 26%. During the mid Late Permian, it decreased to approximately 20%, and then increased once again to approximately 28% in late Late Permian.

3.3 Triassic

During the Triassic, gymnosperms quickly emerged and became dominant. At a global scale, the Triassic was characterized by dry and arid climate, although Middle Triassic was under increased rainfall and occasional humid conditions (Preto et al. 2010). The mass extinction event at the end Permian resulted in a 10 Ma coal-forming gap during the Triassic, when most regions were covered by widespread desert conditions (Kutzbach and Gallimore 1989). The coal was scarce during the Middle Triassic (Retallack et al. 1996).

Coal-bearing strata mainly developed during the Late Triassic in the humid, hot, and rainy southern regions in China. In particular, it occurred in the Xujiahe Formation of Peikucuo Stage (Norian–Rhaetian) in Sichuan, Yunnan, Hubei, Guangdong, and Guizhou (Zhang 1995; Shao et al. 2014). Among those, the strata in Sichuan had the best coal-bearing properties, under coal-forming environments including coastal plains, coastal lake–delta plains, and coastal delta plains (Lu et al. 2008). However, during the same period, northern China was mostly under arid or semi-arid climate. It was only at the end of Late Triassic that coal-bearing strata of river and lake facies were formed in Wayaobao Formation of the Ordos Basin (Tian et al. 2011).

The inertinite abundance varied between the northern and southern China. For example, in the Wayaobao Formation in the north-central Ordos Basin, it was about 24.8%, and was mainly semi-fusinite. However, in southern China, the coal-bearing strata almost covered the entire southwestern regions, with the mean inertinite abundance in coals ranging between 5.8% and 26.3%. In regard to the Maantang Formation of Yazhiliangian Stage (Carnian), the value was 7.9%–19.5% in Zixing (Hunan Province), and 23.2%–28.4% in Sichuan Province, respectively. It varied most in Anyuan Formation of Jiangxi Province, ranging from 1.1% to 21.2% (Table 3).

During the Triassic, the pO_2 recorded a declining trend, from 25% in the early Late Triassic, to 18% at the end Late Triassic, which was the lowest value of the entire Mesozoic Era.

3.4 Jurassic

During the Jurassic, gymnosperms like cycads, conifers, and ginkgo were extremely abundant. The coal-bearing strata mainly developed in the northern and northwestern regions in China during the Early and Middle Jurassic, under a subtropical–warm temperate humid climate (Huang and Hou 1988). The coal-bearing basins were generally dominated by large- and medium-sized inland lake basins; while the coal-forming environments were dominated by alluvial-lake delta systems, followed by lacustrine systems (Li et al. 2018).

The coal-bearing strata during the Early Jurassic were mainly distributed in Badaowan Formation of Yongfeng Stage (Hettangian–Sinemurian) in the Junggar Basin of Xinjiang; Xishanyao Formation of Liuhuanggou Stage (Pliensbachian–Toarcian) in the Tuha and Yili basins, Xinjiang; as well as Xiahuayuan Formation of Shihezi Stage (Pliensbachian–Toarcian) in Hebei and Shandong regions (Shao et al. 2009; Shi et al. 2011). During that period, inertinite abundance in coal deposits varied significantly (Table 4), with mean values of 3.3%–14.8% in Badaowan Formation of Junggar Basin, and 4.7%–49.0% in Xishanyao Formation of Yili Basin.

During the Middle Jurassic, coal was well accumulated in entire northern China (Wu et al. 2008; Qin et al. 2009). Most of the coal-bearing strata were found in Yan'an Formation of Shihezi Stage (Pliensbachian–Toarcian) in the Ordos Basin. In Inner Mongolia, the mean inertinite abundance in coals ranged between 31.9% and 84.0%, with maximum values of up to 86.9% in Longdong Coalfield of Gansu Province. In Xishanyao Formation of Shihezi Stage (Pliensbachian–Toarcian)

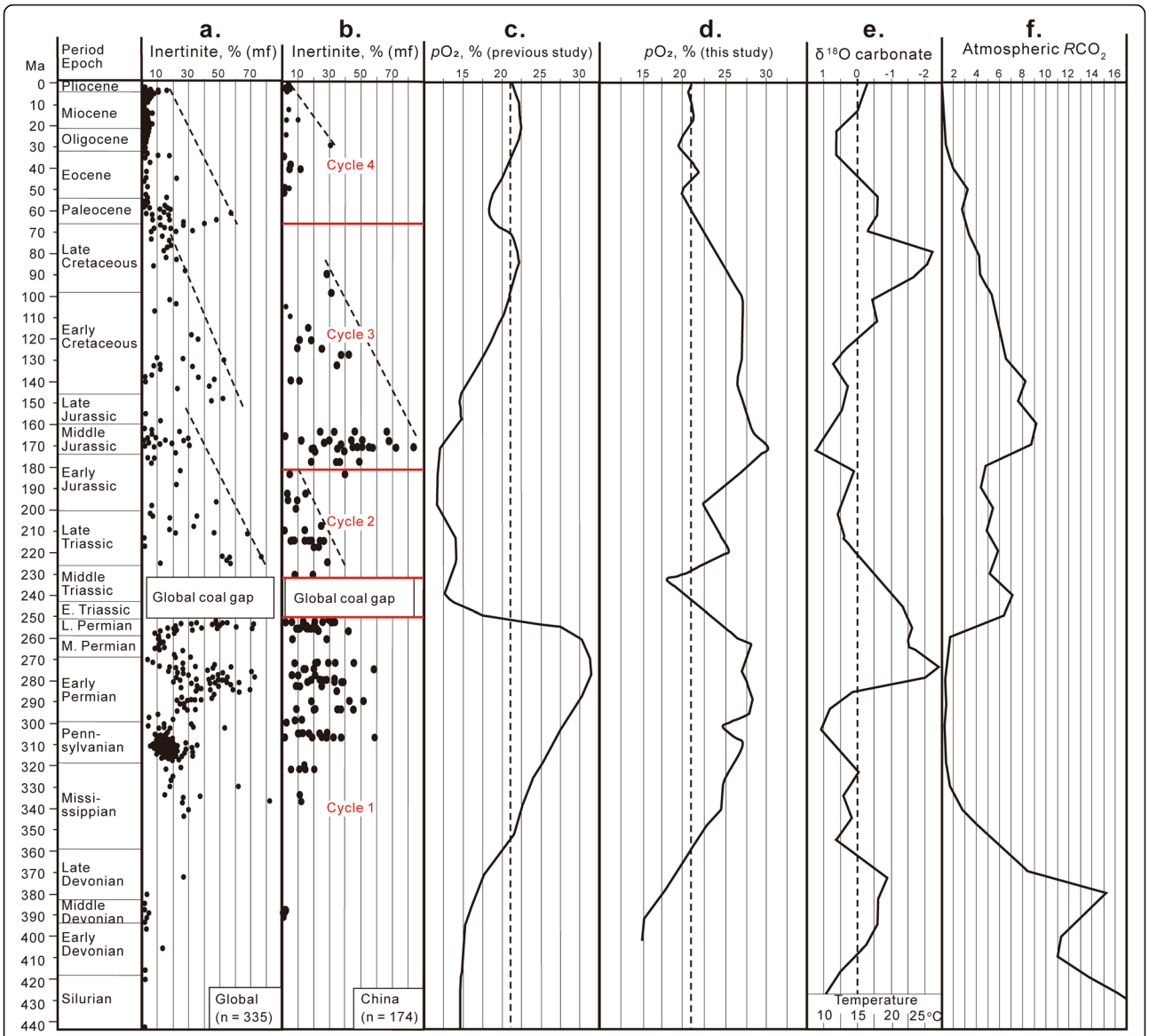

Fig. 2 Summary of inertinite abundance relative to the geological age, atmospheric paleo-oxygen concentration, paleotemperature, and carbon dioxide concentration fluctuations. **a** Geochronological distribution of global inertinite abundance (Diessel 2010). Dashed lines refer to the three repetitions of inertinite abundance from high to low; mf: Mineral-free; **b** Geochronological distribution of inertinite abundance in China. Four major cycles are identified (marked by red lines); **c** Curve of atmospheric paleo-oxygen concentration in previous studies (Berner 1999, 2006; Berner and Kothavala 2001; Ward et al. 2006); **d** Simulation curve of atmospheric paleo-oxygen concentration in this study. Dashed lines in **c** and **d** refer to the pO_2 value of the modern atmosphere (approximately 21%); **e** Variations of the carbonate-hosted oxygen isotopes, and the calculated temperatures (Shaviv and Veizer 2003). Dashed line refers to the base line of oxygen isotope; **f** Changes in atmospheric carbon dioxide concentration. *R*: Ratio of atmospheric CO_2 concentration in geological history compared to the modern atmospheric CO_2 concentration) (Royer et al. 2004)

(Xinjiang), the mean inertinite abundance varied greatly, ranging between 12.2% and 68.8%. In Yaojie Formation of Shihezi Stage (Pliensbachian–Toarcian) in Tianzhu county (Gansu), the value was between 1.1% and 3.4%, which was the lowest values during that period. In Toutunhe Formation of Manasi Stage (Bathonian–Callovian) in Minhe Basin (Qinghai), the value was between 24.0% and 66.5%.

pO_2 changed drastically during the Jurassic compared to earlier periods. Since the Early Jurassic, it began to rise and reached approximately 28% by the end Early Jurassic. During the Middle Jurassic, it rapidly increased

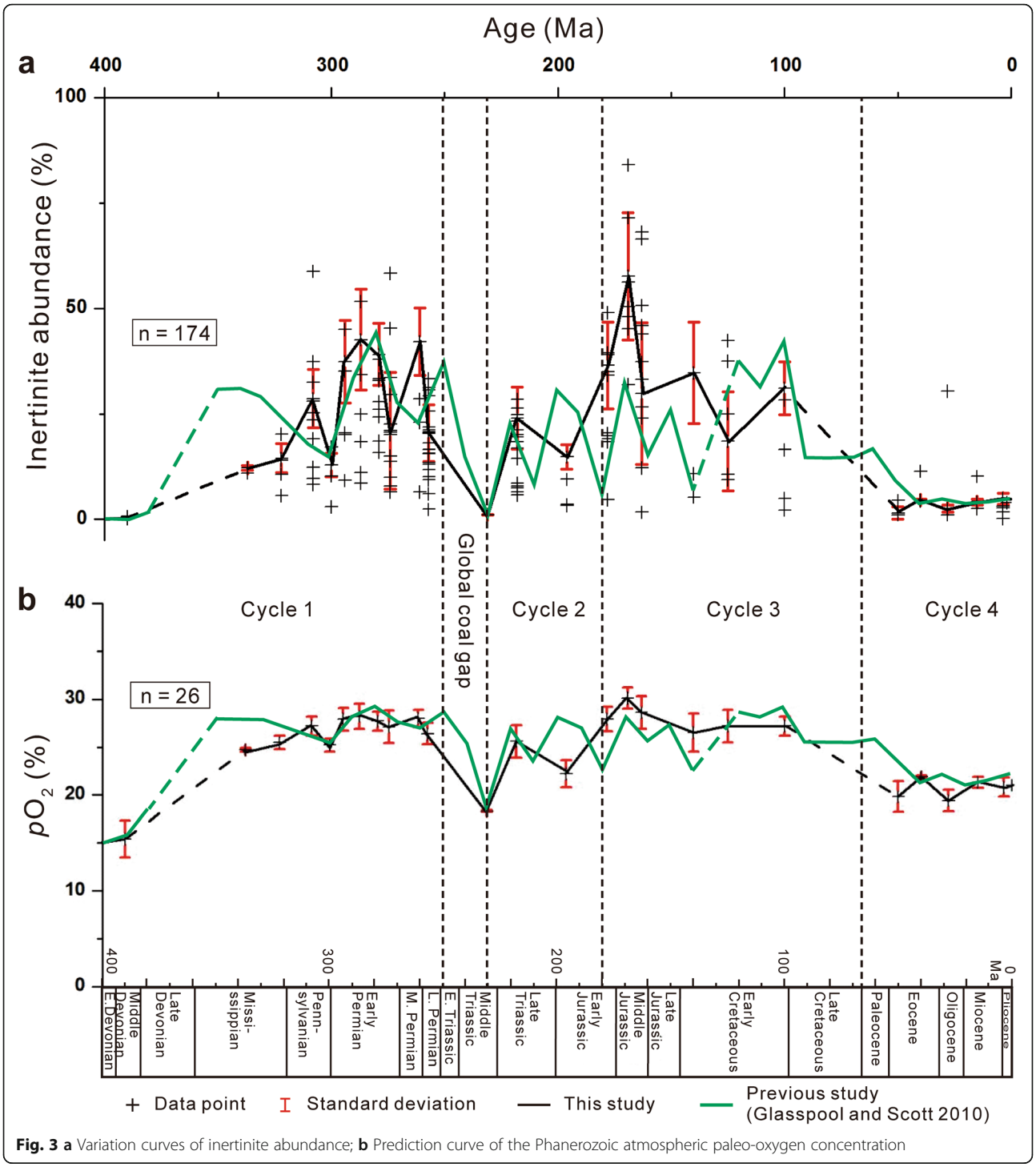

Fig. 3 **a** Variation curves of inertinite abundance; **b** Prediction curve of the Phanerozoic atmospheric paleo-oxygen concentration

to 30% or more, which was the highest value ever recorded and was maintained throughout the Late Jurassic.

3.5 Cretaceous

The Cretaceous was an important period of plant evolution. Angiosperms appeared and flourished, which provided important materials for coal production. During the Early Cretaceous, a series of continental fault basins were formed due to rifting and faulting activities in northeastern China, which provided sites for coal formation (Li et al. 1987). The coal-bearing strata were mainly formed in alluvial fans, fan deltas, lakeside deltas, and lacustrine environments. The coal-rich belts were mainly

located on the sides of main faults near basin margins, with their distribution directions consistent with basin trends (Cai et al. 2011; Shao et al. 2013).

During the Early Cretaceous, coal-bearing strata were mainly distributed in northeastern China, e.g., on the western side of Greater Khingan Mountains and the southern margin of Songliao Basin. They occurred in the Muling Formation, Yixian Formation, and Jiufotang Formation of Rehei Stage (lower Aptian) in Heilongjiang; Fuxin Formation and Shahai Formation of Liaoxi Stage (upper Aptian) in Hebei; and the Huolinhe Formation of Jibei Stage (Berriasian–Hauterivian) and the Yimin Formation of Rehei Stage (Barremian) in Inner Mongolia. The mean inertinite abundance in coal is relatively higher in the west than in the east of northeastern China (Table 5). It varied greatly in some coalfields in western Inner Mongolia, e.g., ranging between 26.1% and 55.8% in Yimin Formation of Jalainur Coalfield, with 42.4% on average. However, this value was relatively low in coalfields in eastern Inner Mongolia. For example, it ranges between 2.2%–16.5% in Fuxin and Tiefa Coalfields of Liaoning Province, and 9.4%–25.0% in Jixi and Hegang Coalfields of Heilongjiang Province. During the Early Cretaceous, pO_2 was slightly lower than that during the Jurassic, which, however, still kept at a relatively high level of approximately 25%.

3.6 Paleogene to Neogene

Since the Cenozoic, evergreen and deciduous broad-leafed plants of modern angiosperms have gradually flourished, which indicated the obvious seasonal climate changes, as well as the rapid development of modern plants which are more adapted to severe climatic conditions (Zhao et al. 1995).

From Paleogene to Neogene, coal-bearing strata mainly developed in small continental basins in the northeastern and southwestern China. The coal-forming processes mainly occurred in the lake and delta marsh environments (Zhang 1995; Li et al. 2018).

During the Paleogene, the coal-bearing basins were mainly distributed to the east of Greater Khingan Mountains and north of Qinling Mountains and southwest of Guangxi. The coal-forming periods include Eocene and Oligocene. (1) The Eocene coal-bearing strata mainly included Hunchun and Shulan formations of Ashantou Stage (Ypresian–Lutetian) in northeastern China; Nadu Formation of Yuanquan Stage in Baise and Nanning basins in Guangxi; and Lijiaya Formation of Yuanquan (Bartonian) in Liangjia Coal Mine in Shandong. (2) The Oligocene coal-bearing strata included the Pinghu Formation of late Caijiachongian Stage (Priabonian) within Xihu Depression of East China Sea, and the Yacheng Formation of Tabenbuluckian Stage (Chattian) in Qiongdongnan Basin. The inertinite abundance in coal was generally low (Table 6), with the mean values ranging between 1.1% and 11.4%. (3) During the Oligocene, a few coal seams developed in Huerjing Formation of Wulanbulagean Stage (Rupelian) in Erlianhot, Inner Mongolia, within which the inertinite abundance was very high, ranging from 23.8% to 38.7%, with a mean value of 30.4%, which was significantly higher than that in other regions during the same period.

During the Neogene, coal-bearing strata were mainly distributed in the Miocene and Pliocene coal basins in the eastern coastal and the southwestern areas of southern China (Zhang 1995), mainly in continental lacustrine basins. The Miocene coal-bearing strata included the Xiaolongtan Formation of Tonggurian Stage (Langhian–Serravallian) in Yunnan Province and the Nanzhuang Formation of Shanwangian Stage (Burdigalian) in the northwestern basins of Taiwan. The Pliocene coal-bearing strata mainly included the Shagou Formation of Mazegouan Stage (Piacenzian) in Shaotong–Qujing Basin of Yunnan. During the Neogene, the total inertinite abundance was relatively low, with the mean value ranging between 0.2% and 10.2%.

During the Quaternary, coal seams were generally developed in Yuanma Formation of Nihewanian Stage (Gelasian–Calabrian) in Tengchong, Yunnan. The inertinite was mainly composed of filamentous bodies and fungi, and was of low abundance (mean value of 4.0%) (Jin and Qin 1989).

Throughout the Cenozoic, pO_2 fluctuated around 21%, which was roughly the same as that in the current atmosphere.

3.7 Inertinite abundance and pO_2 evolution

During the entire Phanerozoic, the abundance and distribution of inertinite in coal varied greatly. In terms of time, there were four major cycles in which the inertinite abundance first increased and then decreased, i.e., during Early Devonian–Late Permian; Late Triassic–Early Jurassic; Middle Jurassic–Late Cretaceous; and Paleogene–Neogene, respectively (Figs. 2, 3a). During these periods, the evolution process of pO_2 also changed a lot (Figs. 2, 3b).

3.7.1 Early Devonian–Late Permian

During the Paleozoic, the inertinite abundance in coal was at a very low level in the Early Devonian. During Middle Devonian, this value was as low as 0.1% in Qujing Formation of Dongganglingian Stage in Yunnan. From Early Carboniferous to Late Permian, accompanied by the unprecedented diversity occurring in the plant kingdom, this value increased rapidly and reached its peak of 58.8% in Taiyuan Formation of

Xiaoyiaoan Stage in Junggar Coalfield, Inner Mongolia. It remained high throughout the Permian, e.g., in Changxing Formation of Changxingian Stage in Guizhou Province. Until Late Permian, it slowly decreased to 30.7%. From Devonian to Permian, the pO_2 kept increasing and reached a maximum value of approximately 29% during the Middle Permian. Throughout Permian–Triassic, the pO_2 values fluctuated several times. However, prior to the Early Triassic, the pO_2 values had rapidly decreased to 23%.

3.7.2 Late Triassic–Early Jurassic

During the Mesozoic, the inertinite abundance in coal-bearing strata of China was quite different from that of the Paleozoic. During the early Late Triassic, it rapidly decreased to 1.1%, the lowest value of the entire Phanerozoic, in Anyuan Formation of Peikucuo Stage in Leping (Pingxiang, Jiangxi). Immediately after the global coal gap of the Early and Middle Triassic, the inertinite abundance of the Late Triassic increased rapidly until reaching the same level as before the Early Triassic, with the peak value of 28.4% in Sichuan. From Late Triassic to Early Jurassic, the value decreased rapidly, only 4.7% in Xishanyao Formation of Liuhuanggou Stage in Tuha Basin (Xinjiang). Correspondingly, during the early Late Triassic, pO_2 was at the lowest level of only 18%, which, however, increased rapidly since the Early Jurassic, reaching up to 26% by the end of Early Jurassic.

3.7.3 Middle Jurassic–Late Cretaceous

During the entire Jurassic, the inertinite abundance displayed an increasing trend. It was not high at the Early Jurassic, but increased rapidly since the early Middle Jurassic, and reached 84%, i.e., the maximum value of the entire geological history at Yan'an Formation of Shihezi Stage in Gansu Province. However, the value significantly decreased since the Early Cretaceous. By the Late Cretaceous, it reduced to 28.3% in Fuxin Formation of Liaoxi Stage in Wanquan Coalfield, Hebei Province. Correspondingly, from Middle Jurassic to Late Cretaceous, pO_2 also changed greatly, which first increased to over 30% during the Middle Jurassic, and then slowly decreased but still remained as over 25%.

3.7.4 Paleogene–Neogene

The inertinite abundance in coal-bearing strata decreased during the Cenozoic when compared with prior periods, but was relatively stable. However, this value increased since the beginning of the Paleocene. During Oligocene, it reached 30.4%, the maximum value of the entire period, in the Huerjing Formation of Wulanbulagean Stage in Erenhot, Inner Mongolia, and then decreased again. During Neogene, it decreased to 1.8% in Shagou Formation of Mazegouan Stage. During the entire Cenozoic, pO_2 did not change significantly, remaining between 20% and 22%, which was equivalent to the current oxygen levels in the atmosphere.

4 Genetic analysis and comparison of inertinite abundance and pO_2 characteristics during different coal-forming periods

China has experienced many coal-forming periods over a long span of time, The data generated from the coal deposits are important for the global study on inertinite abundance and pO_2 characteristics in coal-bearing strata. In this study, by examining the characteristics of inertinite abundance in China's coal-bearing strata during each coal-forming period, and comparing the results with worldwide researches conducted by Diessel (2010), it was found that the basic trends were the same (Fig. 2). For example, during the Early Paleozoic, coal-forming processes were weak, and the inertinite abundance in coal was relatively low. Then, during the Late Paleozoic, this abundance showed regular increases or decreases on a global scale during different coal-forming periods. These trends were manifested as the high inertinite abundance from Late Carboniferous to Early Permian. The Middle Permian values were lower, and there was a rapid increase again during the Late Permian. It is also determined that from the Mesozoic to the Cenozoic, and from the Early Triassic to the Middle Triassic, the inertinite abundance changed greatly. There were generally three repetitions of inertinite abundance form high to low, which covered the time span of: (1) from Late Triassic to Early Jurassic; (2) from Middle Jurassic to Late Cretaceous; and (3) from Paleogene to Neogene, respectively. However, differing from the global research results of Diessel (2010), the inertinite abundance of the Middle Jurassic coal in northern and northwestern China was very high, reaching the peaks of each of the coal-forming periods. The atmospheric pO_2 in each of the coal-forming periods, which was simulated by the inertinite abundance in coal, also displayed corresponding characteristics (Fig. 2).

4.1 Early Devonian–Late Permian

During the Paleozoic in China, the inertinite abundance in coal-bearing strata displayed a trend of alternating increase and decrease. This was particularly obvious in regard to the high inertinite abundance from Late Carboniferous to Early Permian, showing low values during Middle Permian and rapid increase again during Late Permian. The variations were consistent with those observed for the global coal deposits, indicating that the formation of inertinite in coal during that period was significantly influenced by global factors (for example, atmospheric paleo-oxygen concentrations), which went

beyond the influence of regional environments and their specific flora (Diessel 2010).

During the Early Carboniferous, the existing plants mainly grew in coastal lowland areas, and the climatic differentiation and palaeogeographical isolation were not obvious. In Late Carboniferous, latitudinal zonation occurred in the plant kingdom in order to adapt to climatic differentiation (Liu and Quan 1996). In the Carboniferous, coal deposits were mainly distributed in the southern continental Laurasia–Russia and the western Baltic Plate under tropical environments. Coal deposits were also located in the northwestern regions of continental Gondwana in Africa; and the northern parts of China and the Siberian Plate of the northern temperate zones. The first few regions were tropical year-round moist plant zones, while the Siberian Plate belonged to the temperate plant zones (Li and Jiang 2013). During the Carboniferous, terrestrial plants were diverse and vascular systems rapidly developed. The lignin tissues of plants were prone to smoldering, which was conducive to forming inertinite (Diessel 2010). The climatic zoning and geographical division of the plants were still similar to those of the Carboniferous (Li and Jiang 2013). During the Late Permian, the Earth's vegetation was rich in lignin and was more prone to smoldering than full combustion (Robinson 1989). The tendency of lignin to form coke (for example, inert components) in the pyrolysis process may have contributed greatly to the increases in the content of inertinite components at the end Permian (Diessel 2010). Furthermore, during the Late Permian, local volcanic eruptions in northern China triggered massive wildfires (Zhao et al. 2010), which also contributed to the increases of inertinite abundance in China's coal deposits.

There is a close relationship between the oxygen content in atmosphere and the metabolism of plants and animals (Robinson 1989). The distribution of oxygen within the atmosphere of an area is particularly related to the variations in abundance of inertinite (Berner 2006; Ward et al. 2006). The growth of forest vegetation, as well as plant assimilation and transpiration led to the removal of a large amount of carbon dioxide from the atmosphere (Diessel 2010). The carbon extracted from atmospheric carbon dioxide was photosynthesized into plants, and much of that became buried and stored in the form of fossil fuel. Marshall et al. (2020) found a large number of mutant plant sporopollen based on mass extinction events during the Devonian–Carboniferous. The variation of plant debris reflectivity distribution indicates a higher charcoal content, indicating that atmospheric oxygen does not decrease. During the Carboniferous–Permian coal-forming periods, the pO_2

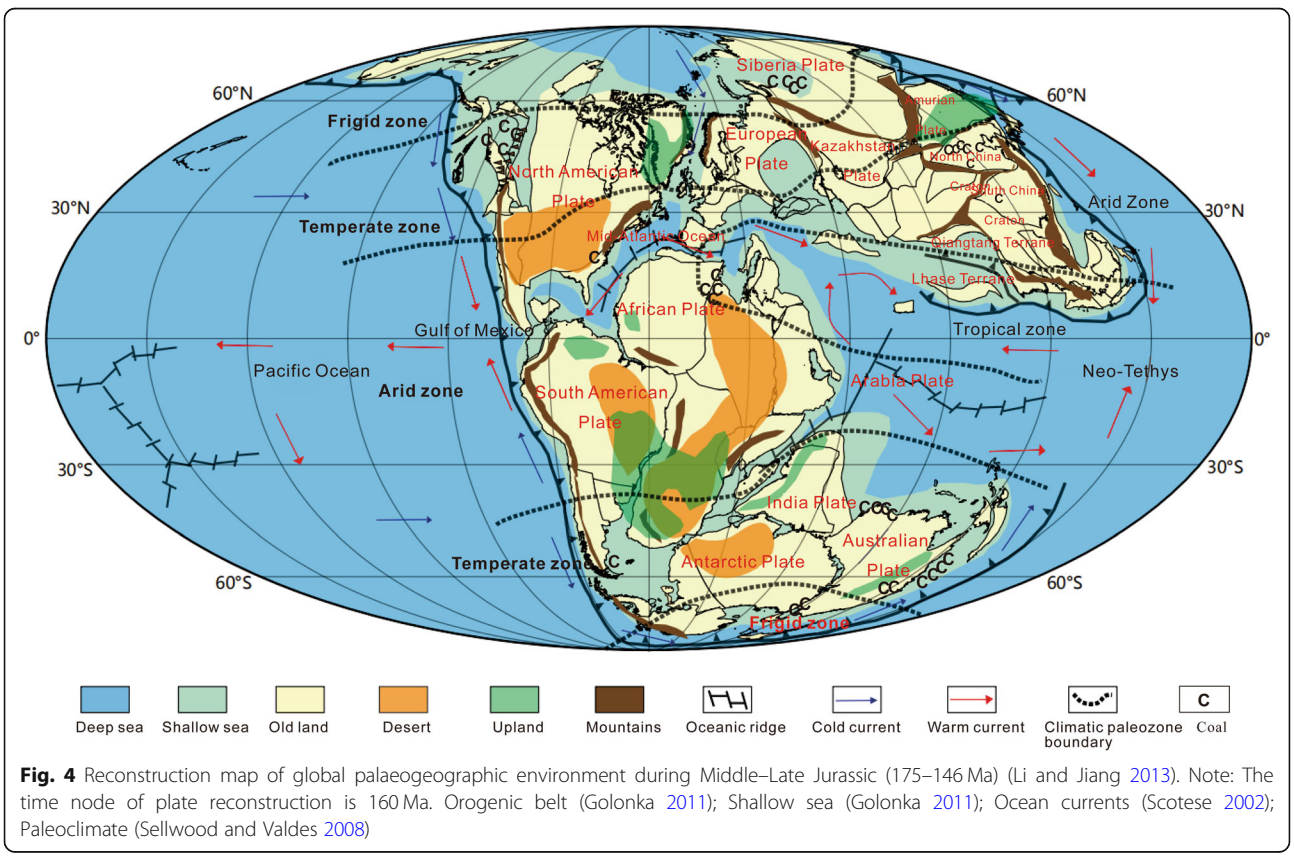

Fig. 4 Reconstruction map of global palaeogeographic environment during Middle–Late Jurassic (175–146 Ma) (Li and Jiang 2013). Note: The time node of plate reconstruction is 160 Ma. Orogenic belt (Golonka 2011); Shallow sea (Golonka 2011); Ocean currents (Scotese 2002); Paleoclimate (Sellwood and Valdes 2008)

changed greatly. The diversity of terrestrial plants increased significantly during the Early Carboniferous, resulting in a continuous increase in paleo-oxygen concentrations throughout the Carboniferous. Until the Mesozoic, the pO_2 remained at or above 26%, which was consistent with the predictions based on plant carbon isotopic fractionation (Lenton and Watson 2000). During the Middle Permian, the pO_2 first decreased, and then fluctuated. However, it continued to remain at high levels. The aforementioned fluctuation pattern of the pO_2 was very similar to the bimodal distribution model of pO_2 established in previous study (Bergman et al. 2004). Diessel (2010) found a relationship between the high inertinite content, the high atmospheric oxygen and low atmospheric carbon dioxide levels in Late Paleozoic. However, the inertinite abundance was found to be more complex than the relatively undifferentiated oxygen curves and closer to the δO^{18} paleotemperature model.

In previous comprehensive analyses, the global coal-forming plant types, sedimentary environments, and the climatic zones of the Paleozoic were found to be relatively stable. The inertinite abundance in global coal deposits were remarkably consistent, and were mainly controlled by the changes of global atmospheric pO_2. The differences in the abundance and dispersion degrees of inertinite in coal deposits located in different regions also reflected the fact that they had been influenced by such secondary factors as climate, deposition, and structure.

4.2 Late Triassic–Early Jurassic

The end-Permian mass extinction (Virgili 2008) halted coal formation worldwide for approximately 10 Ma. This is widely believed to result from the chain reaction caused by eruption of Siberian igneous provinces (Diessel 2010; Zhao et al. 2020). The coal seams appeared again in the Late Triassic with high inertinite abundance. After that period, the inertinite abundance displayed a trend of gradually decreasing until it reached its lowest point in the middle to late parts of the Early Jurassic.

The geographical distributions of global supercontinents determined the climatic and environmental characteristics of various regions during the Triassic. For example, from the Late Permian, the glaciers gradually began to disappear, and as the sea level rose, global warming occurred. The majority of Pangaea was located in arid and tropical zones, while the remainder was located in temperate zones. The Late Triassic coal-forming regions were mainly distributed in the arid and tropical climatic zones located around the Northern Hemisphere's Paleotethys Ocean (Li and Jiang 2013). From the Late Triassic to Early Jurassic, extensive volcanic activities in the central Atlantic magma province led to the release of large amounts of carbon dioxide and/or methane. This had resulted in extreme greenhouse effects, with wetter climatic conditions and increased storm and lightning activities (Petersen and Lindström 2012). These storm and lightning events frequently led to a large number of fires (Belcher et al. 2010), which produced high concentrations of charcoal (inertinite), resulting in a relatively high abundance of inertinite in the coal deposits.

Compared to the Permian, the records of Triassic charcoal are actually very sparse, reflecting the relatively low oxygen content in the atmosphere at that time. According to the simulations of inertinite abundance during the Late Triassic, the atmospheric pO_2 during that period had decreased from approximately 25% to 18% in China, globally even dropped below 13% (Berner 2002, 2005). Paleoredox and phosphorus speciation data from the ocean depth profile of Svalbard were for this time provided by Schobben et al. (2020). Large areas of the ocean experienced hypoxia prior to the Permian–Triassic boundary and caused some species to disappear before the major extinction at the Permian–Triassic boundary (Huey and Ward 2005). A large amount of CO_2 was released into atmosphere by the explosions in Siberian large igneous provinces, which subsequently led to decrease in the pO_2 (Zhao et al. 2020). However, the terrestrial plants caused rise in pO_2 in the atmosphere significantly (Rimmer et al. 2015). The low pO_2 is also reflected by the slow recovery of land vegetation following the Permian–Triassic mass extinction event.

4.3 Middle Jurassic–Late Cretaceous

From the late Early Jurassic to the Late Cretaceous, the abundance of inertinite in China's coal had displayed a trend of gradual decrease. Previous studies on a global scale suggested that the inertinite abundance in coal decreased from the Late Triassic to Late Jurassic (Diessel 2010). The coal forming process during the middle and late Late Jurassic in China was not favourable. During the Late Cretaceous, both the coal-forming intensity and the abundance of the inertinite in coal decreased gradually.

During the Jurassic, coal was mainly developed in the north and south latitudes 40° polar region. The climate at that time was dominated by temperate type, whereas frigid climate zone was distributed in the northern of Siberia. The development and distribution of coal seams had symbiotic relationships with the survival of plants at that time. The plants surviving near the equator were the most singular, with conifers and cycads mainly developing into scattered forests. In the middle latitudes, conifers, cycads, and ferns flourished with large numbers of species and genera. However, compared with the equatorial regions, the higher latitudes mainly included

broad-leafed plants such as *Ginkgo biloba*. From a global perspective, only the coal-forming areas in northern and northwestern China were considered to be located in inland arid climatic zones. Meanwhile, the coal-forming areas in other regions were mainly located in the coastal areas of temperate zones, and a few in the coastal areas of cold zones (Li and Jiang 2013) (Fig. 4). For example, the Middle Jurassic Yan'an Formation in Ordos Basin was formed under relatively dry climatic conditions (Huang et al. 2010). The surfaces of peat bogs during coal-forming periods were under oxidative conditions for long periods of time (Zhang and Wu 1996; Chen et al. 2013). The simultaneous occurrences of charcoal fragments and high concentrations of pyrolytic paths in the Yan'an Formation coal seams of the Ordos Basin provided evidence of peatland wildfires. The cycles of peatland wildfires were caused by seasonal changes driven by the changes in rainfall. The low reflectivity of inertinites in all of the coal seams may have resulted from low-temperature surface peatland wildfires with relatively high atmospheric paleo-oxygen concentrations of approximately 29% (Zhang et al. 2020). The pO_2 in the Jurassic global atmosphere should have been consistent and did not vary from place to place. The differences in climatic zones, plant types, and sedimentary environments had significant impacts on the inertinite abundance in coal deposits. This may also have been an important reason why the inertinite abundance in the Jurassic coal in China was much higher than that in other parts of the world.

During the late Early Jurassic, the pO_2 increased rapidly (~ 28%); reached its maximum value (> 30%); and then gradually decreased (~ 25%). Previous studies suggested that the pO_2 in the atmosphere had decreased to approximately 12% during the Early and Middle Jurassic (Berner 1999, 2006; Berner and Kothavala 2001; Ward et al. 2006). In fact, some researchers have also questioned the effectiveness of such lower atmospheric pO_2. Therefore, based on combustion experiments under the fully-controlled conditions of various materials, it is now believed that at least a 15% atmospheric pO_2 was required for inertinite to produce the Mesozoic wildfires (Belcher and McElwain 2008).

During the Cretaceous, the abundance of inertinite in coal deposits fluctuated, which was closely related to the climatic conditions of the same period. Also, during the Cretaceous, a high-temperature environment existed throughout the world, with the temperate zones in the Northern Hemisphere reaching 60° north latitude and in the Southern Hemisphere reaching 70° south latitude. Therefore, with intense volcanic activities around the world, the atmospheric carbon dioxide content reached the highest level in history, which exacerbated the greenhouse effects and played a key role in the prosperity of terrestrial animals and plants. The coal-forming regions of the world during Cretaceous were mainly located in the tropical and subtropical climatic zones between approximately 30° and 60° north latitudes in the Northern Hemisphere, and some were located within the cold zones where the coal mainly formed in coastal environments and subordinately in the inland areas (Li and Jiang 2013). The climate of the Cretaceous changed frequently, during which there were significant drought or rainfall events (Spicer 2003; Belcher and McElwain 2008; Belcher et al. 2010; Brown et al. 2012) which affected the abundance of inertinite in coal. Early Cretaceous anoxic event (Huang et al. 2008) had profound effects on the atmosphere–ocean system, as well as the accompanying global cooling and the enhancement of the ocean oxidative capacity. Boudinot and Sepúlveda (2020) believed that the Mid-Cretaceous oceanic anoxic event would lead to a decrease in pCO_2 and an increase in pO_2 in the atmospheric and oceanic system, and trigger mountain fires, indicating that the oxygen content in the Mid-Cretaceous was not low. Atmospheric pO_2 was calculated by simulating the abundance of inertinite in coal during this period. The atmospheric pO_2 in the Early Cretaceous was high and displayed a gradually decreasing trend, which was significantly higher than the previous studies (Berner 1999, 2006; Berner and Kothavala 2001; Ward et al. 2006).

4.4 Paleogene–Neogene

From the beginning of the Paleogene to the end of the Neogene, the abundance of inertinite increased slightly after the Paleocene, but still remained at a low level. Although some researchers reported forest fires during that period, the heavy rainfall events during the early Oligocene may have mitigated the impacts.

5 Discussion

The inertinite abundance in global coal during the Paleozoic displayed a fluctuating trend, particularly during the Late Carboniferous to Early Permian. It was higher in the Middle Permian coal, lower in the Late Permian coal, and more concentrated in the global coal. These findings indicated that the formation of inertinite during the Paleozoic was significantly influenced by global factors (such as atmospheric paleooxygen concentrations) (Diessel 2010), which went beyond the influence of regional environmental conditions and specific flora (Teichmüller 1952; Snyman 1961; Falcon 1975).

From the Mesozoic to the Cenozoic, the abundance of inertinite in coal changed greatly following the coal discontinuity which occurred from the Early to Middle Triassic. The general trend was that the inertinite abundance in the coal deposits repeated three times respectively, from high to low. On a global scale, the three

replications were the Late Triassic to Late Jurassic; Late Jurassic to Late Cretaceous; and Late Cretaceous to Holocene (Diessel 2010; Glasspool and Scott 2010). In China, the three repetitions comprised the Late Triassic to Early Jurassic; Middle Jurassic to Late Cretaceous; and Paleogene to Neogene. The difference lies in the fact that the abundance of inertinite during the Middle to Late Jurassic in China was much higher than that in other parts of the world (Wang et al. 2019).

Diessel (2010) conducted a systematic study regarding the stratigraphic characteristics of global inertinite. The research results generally supported the theory that the global atmospheric pO_2 was the main controlling factor for the abundance of inertinite in global coal. In addition, the influences of climate conditions, sedimentary environments, differential subsidence, and other factors were believed to have led to regional and local changes in the abundance of inertinite in coal. This study also supported those viewpoints as a whole, and suggests that the global atmospheric pO_2 was the main controlling factor of the abundance of inertinite in global coal. During Paleozoic, due to the relatively single and stable coal-forming climatic zones, plant types, and sedimentary environmental conditions, the inertinite abundance in coal deposits was very obvious in response to the atmospheric pO_2 (Scott 2000, 2002; Glasspool et al. 2015; Yan et al. 2019). However, since the Mesozoic, due to the diversification and complexity of coal-forming climatic zones, plant differentiation, coal-forming sedimentary environmental conditions, tectonic activities, sea level changes, and so on (Vail et al. 1977; Hunt and Smyth 1989), the local and dramatic changes in the abundance of inertinite in coal may have sometimes exceeded the influence of global atmospheric pO_2.

6 Conclusions

In this investigation, the coal during each coal-forming period in China was taken as the research objects. The abundance of inertinite in coal during each coal-forming period was systematically analyzed. The atmospheric pO_2 characteristics during the coal-forming periods were successfully simulated and calculated. The following conclusions were reached in this study:

1) The systematic analysis of a large volume of data reveals the inertinite abundance and its evolution during the Phanerozoic coal-forming periods in China. Four major cycles were identified, in which the inertinite abundance first increased and then decreased. These are: Early Devonian to Late Permian; Late Triassic to Early Jurassic; Middle Jurassic to Late Cretaceous; and Paleogene to Neogene, respectively.
2) Based on a large amount of statistical data regarding the inertinite abundance in coal during each of the coal-forming periods in China, the atmospheric pO_2 characteristics of each of the coal-forming periods were simulated. The evolution curves of atmospheric pO_2 during each coal-forming period were quantitatively constructed, which provided a certain reference for further research regarding atmospheric pO_2 in geological history.
3) Through comparative studies on a global scale, the characteristics and evolution of the inertinite abundance and atmospheric pO_2 in various coal-forming periods were further supplemented and improved, particularly in regard to the Jurassic.
4) It was further clarified in this study that the global atmospheric pO_2 was the main controlling factor of the inertinite abundance in global coal deposits. The relationship between the inertinite abundance in Paleozoic coal to the atmospheric pO_2 is established. However, since the Mesozoic, besides the diversity and complexity of coal-forming climatic zones, plant differentiation, coal-forming sedimentary environmental conditions, tectonic activities, and wildfire events, regional factors might have influenced global atmospheric pO_2.

Abbreviations

pO_2: Paleo-oxygen concentration; I_{AVG}, %: Mean inertinite abundance; N: Number of samples; R: Percentage range (min–max), %; S: Standard deviation

Acknowledgements

We thank the editors and reviewers for their constructive comments to improve the manuscript.

Authors' contributions

DDW proposed the main academic ideas of the manuscript, and participated in guiding the writing of the whole manuscript. LSY is mainly responsible for collecting data of inertinite abundance in coal in various geological periods, screening and processing data, and calculating paleooxygen content. LYS mainly makes a comprehensive analysis of the geological origin and evolution of the high inertinite abundance in coal. DWL mainly analyzes the development and distribution characteristics of inertinite abundance in coal in various geological periods. HYL mainly analyzes the reasons for the abnormally high inertinite abundance in Jurassic coal. SW mainly analyzes the geological reasons of inertinite abundance in Cenozoic coal. GQD assists in collecting geological data and drawing maps. All authors read and approved the final manuscript.

Funding

This work was supported by the National Natural Science Foundation of China (41972170, 41772096, 41402086), the Natural Science Foundation of Shandong Province (ZR2019MD021), and the SDUST Research Fund (2018TDJH101).

Availability of data and materials

All data generated or analyzed during this study are included in the manuscript.

Declarations

Competing interests

The authors declare that they have no competing interests.

Author details

[1]College of Earth Science and Engineering, Shandong University of Science and Technology, Qingdao 266590, Shandong Province, China. [2]College of Geoscience and Surveying Engineering, China University of Mining and Technology (Beijing), Beijing 100083, China.

Received: 19 July 2020 Accepted: 7 April 2021
Published online: 20 May 2021

References

All China Commission of Stratigraphy. 2015. *Chinese stratigraphic guide and instruction book, 2014 Edition*. Beijing: Geological Publishing House (in Chinese). http://dcw.cags.ac.cn/.

Belcher, C.M., L. Mander, G. Rein, F.X. Jervis, M. Haworth, S.P. Hesselbo, I.J. Glasspool, and J.C. McElwain. 2010. Increased fire activity at the Triassic/Jurassic boundary in Greenland due to climate-driven floral change. *Nature Geoscience* 3 (6): 426–429. https://doi.org/10.1038/ngeo871.

Belcher, C.M., and J.C. McElwain. 2008. Limits for combustion in low O_2 redefine paleoatmospheric predictions for the Mesozoic. *Science* 321 (5893): 1197–1200. https://doi.org/10.1126/science.1160978.

Bergman, N.M., T.M. Lenton, and A.J. Watson. 2004. COPSE: A new model of biogeochemical cycling over Phanerozoic time. *American Journal of Science* 304 (5): 397–437. https://doi.org/10.2475/ajs.304.5.397.

Berner, R.A. 1999. Atmospheric oxygen over Phanerozoic time. *Proceedings of the National Academy of Sciences of the United States of America* 96 (20): 10955–10957. https://doi.org/10.1073/pnas.96.20.10955.

Berner, R.A. 2002. Examination of hypotheses for the Permo–Triassic boundary extinction by carbon cycle modeling. *Proceedings of the National Academy of Sciences of the United States of America* 99 (7): 4172–4177. https://doi.org/10.1073/pnas.032095199.

Berner, R.A. 2005. The carbon and sulfur cycles and atmospheric oxygen from Middle Permian to Middle Triassic. *Geochimica et Cosmochimica Acta* 69 (13): 3211–3217. https://doi.org/10.1016/j.gca.2005.03.021.

Berner, R.A. 2006. GEOCARBSULF: A combined model for Phanerozoic atmospheric O_2 and CO_2. *Geochimica et Cosmochimica Acta* 70 (23): 5653–5664. https://doi.org/10.1016/j.gca.2005.11.032.

Berner, R.A., Kothavala, Z., 2001. GEOCARB III: A revised model of atmospheric CO_2 over Phanerozoic time. IGBP PAGES/World Data Center for Paleoclimatology Data Contribution Series. *# 2002–051*.

Boudinot, F.G., and J. Sepúlveda. 2020. Marine organic carbon burial increased forest fire frequency during oceanic anoxic event 2. *Nature Geoscience* 13 (10): 693–698. https://doi.org/10.1038/s41561-020-0633-y.

Brown, S.A.E., A.C. Scott, I.J. Glasspool, and M.E. Collinson. 2012. Cretaceous wildfires and their impact on the earth system. *Cretaceous Research* 36 (2): 162–190. https://doi.org/10.1016/j.cretres.2012.02.008.

Bustin, R.M. 1997. Cold temperate peats and coals: Their sedimentology and composition. In *Late Glacial and Postglacial Environmental Changes: Quaternary, Carboniferous–Permian and Proterozoic*, ed. I.P. Martini. New York: Oxford University Press.

Cai, H.A., B.F. Li, L.Y. Shao, D.B. Xu, K. Shao, and Y.Y. Zhou. 2011. Sedimentary environments and coal accumulation patterns of the Lower Cretaceous Shahai Formation in Fuxin Basin, Liaoning Province. *Journal of Palaeogeography (Chinese Edition)* 13 (5): 481–491 (in Chinese with English abstract).

Chang, J.L., and Q. Gao. 1993. A preliminary study of Carbo-Permian paleoclimate in Shanxi Province. *Journal of Stratigraphy* 17 (2): 154–160 (in Chinese).

Chen, X.W., S.H. Li, Q.X. Fang, T. Alimujiang, B.Q. Li, and F.H. Ma. 2013. Analysis on sequence stratigraphy based on Jurassic outcrop in Kuqa-Bai coalfield. *Xinjiang Geology* 31 (1): 77–82 (in Chinese with English abstract).

Corrêa-da-Silva, Z.C., and M. Wolf. 1980. O poder refletor como parâmetro para a determinação do grau de carbonificação dos carvões gonduânicos do sul do Brasil. *Pesquisas* 13: 35–42.

Dai, S.F., C.L. Chou, M. Yue, K.L. Luo, and D.Y. Ren. 2005. Mineralogy and geochemistry of a Late Permian coal in the Dafang coalfield, Guizhou, China: Influence from siliceous and iron-rich calcic hydrothermal fluids. *International Journal of Coal Geology* 61 (3–4): 241–258. https://doi.org/10.1016/j.coal.2004.09.002.

Dai, S.F., D.X. Han, and C.L. Chou. 2006. Petrography and geochemistry of the Middle Devonian coal from Luquan, Yunnan Province, China. *Fuel* 85 (4): 456–464. https://doi.org/10.1016/j.fuel.2005.08.017.

Dai, S.F., D. Li, C.L. Chou, L. Zhao, Y. Zhang, D.Y. Ren, Y.W. Ma, and Y.Y. Sun. 2008. Mineralogy and geochemistry of boehmite-rich coals: New insights from the Haerwusu surface mine, Jungar coalfield, Inner Mongolia, China. *International Journal of Coal Geology* 74 (3–4): 185–202. https://doi.org/10.1016/j.coal.2008.01.001.

Dai, S.F., D.Y. Ren, X.Q. Hou, and L.Y. Zhao. 2003. Geochemical and mineralogical anomalies of the Late Permian coal in the Zhijin coalfield of Southwest China and their origin. *International Journal of Coal Geology* 55 (2–4): 117–138. https://doi.org/10.1016/S0166-5162(03)00083-1.

Diessel, C.F.K. 2010. The stratigraphic distribution of inertinite. *International Journal of Coal Geology* 81 (4): 251–268. https://doi.org/10.1016/j.coal.2009.04.004.

Falcon, R.M.S. 1975. Application of palynology in sub-dividing the coal-bearing formations of the Karoo sequence in southern Africa. *South African Journal of Science* 71 (11): 336–344.

Falcon, R.M.S. 1989. Macro- and micro-factors affecting coal-seam quality and distribution in southern Africa with particular reference to the no. 2 seam, Witbank coalfield, South Africa. *International Journal of Coal Geology* 12 (1-4): 681–731. https://doi.org/10.1016/0166-5162(89)90069-4.

Glasspool, I.J., D. Edwards, and L. Axe. 2006. Charcoal in the Early Devonian: A wildfire-derived Konservat–Lagerstätte. *Review of Palaeobotany and Palynology* 142 (3–4): 131–136. https://doi.org/10.1016/j.revpalbo.2006.03.021.

Glasspool, I.J., and A.C. Scott. 2010. Phanerozoic concentrations of atmospheric oxygen reconstructed from sedimentary charcoal. *Nature Geoscience* 3 (9): 627–630. https://doi.org/10.1038/ngeo923.

Glasspool, I.J., A.C. Scott, D. Waltham, N. Pronina, and L.Y. Shao. 2015. The impact of fire on the Late Paleozoic Earth system. *Frontiers in Plant Science* 6: 756. https://doi.org/10.3389/fpls.2015.00756.

Golonka, J. 2011. Phanerozoic palaeoenvironment and palaeolithofacies maps of the Arctic region. *Geological Society, London, Memoirs* 35 (1): 79–129. https://doi.org/10.1144/M35.6.

Han, D.X. 1996. *Coal Petrology of China*. Xuzhou: China University of Mining and Technology Press (in Chinese).

Han, D.X., Y.B. Wang, B. Quan, and D.S. Cheng. 1993. The evolution of Devonian coal accumulation in China. *Coal Geology and Exploration* 21 (5): 1–6 (in Chinese with English abstract).

Hower, J.C., J.M.K.O. Keefe, C.F. Eble, A. Raymond, B. Valentim, T.J. Volk, A.R. Richardson, A.B. Satterwhite, R.S. Hatch, J.D. Stucker, and M.A. Watt. 2011. Notes on the origin of inertinite macerals in coal: Evidence for fungal and arthropod transformations of degraded macerals. *International Journal of Coal Geology* 86 (2–3): 231–240. https://doi.org/10.1016/j.coal.2011.02.005.

Huang, K.X., and E.K. Hou. 1988. Paleoclimate of Early and Middle Jurassic in northern Ordos Basin. *Coal Geology and Exploration* 16 (3): 3–8 (in Chinese).

Huang, W.H., W.H. Ao, C.M. Weng, X.L. Xiao, D.M. Liu, X.Y. Tang, P. Chen, Z.G. Zhao, H. Wan, and B. Finkelman. 2010. Characteristics of coal petrology and genesis of Jurassic coal in Ordos Basin. *Geoscience* 24 (6): 1186–1197 (in Chinese with English abstract).

Huang, Y.J., C.S. Wang, and J. Gu. 2008. Cretaceous oceanic anoxic events: Research progress and forthcoming prospects. *Acta Geologica Sinica* 82 (1): 21–30 (in Chinese with English abstract).

Hudspith, V., A.C. Scott, M.E. Collinson, N. Pronina, and T. Beeley. 2012. Evaluating the extent to which wildfire history can be interpreted from inertinite distribution in coal pillars: An example from the Late Permian, Kuznetsk Basin, Russia. *International Journal of Coal Geology* 89: 13–25. https://doi.org/10.1016/j.coal.2011.07.009.

Huey, R.B., and P.D. Ward. 2005. Hypoxia, global warming, and terrestrial Late Permian extinctions. *Science* 308 (5720): 398–401. https://doi.org/10.1126/science.1108019.

Hunt, J.W. 1989. Permian coals of eastern Australia: Geological control of petrographic variation. *International Journal of Coal Geology* 12: 589–634. https://doi.org/10.1016/0166-5162(89)90066-9.

Hunt, J.W., and M. Smyth. 1989. Origin of inertinite-rich coals of Australian cratonic basins. *International Journal of Coal Geology* 11 (1): 23–46. https://doi.org/10.1016/0166-5162(89)90111-0.

Jin, K.L., and Y. Qin. 1989. Coal petrology and anomalous coalification of middle and Late Pleistocene peat and soft brown coal from the Tengchong Basin, western Yunnan, People's Republic of China. *International Journal of Coal Geology* 13: 143–170.

Kutzbach, J.E., and R.G. Gallimore. 1989. Pangaean climates: Megamonsoons of the megacontinent. *Journal of Geophysical Research* 94 (D3): 3341–3357. https://doi.org/10.1029/JD094iD03p03341.

Lenton, T.M., and A.J. Watson. 2000. Redfield revisited: 2. What regulates the oxygen content of the atmosphere? *Global Biogeochemical Cycles* 14 (1): 249–268. https://doi.org/10.1029/1999GB900076.

Li, B.F., X.D. Wen, X.F. Kang, G.D. Li. 1997. The application of high resolution sequence stratigraphy to paralic and terrestrial coal-bearing strata: Two case studies from western North China Paleozoic Basin and the Tulufan-Hami Jurassic Basin. In: Q. Yang, Proceedings of the 30th International Geological Congress. Geology of Fossil Fuels Coal. 18 (B): 1–19.

Li, J.H., and H.F. Jiang. 2013. *Atlas of Global Paleoplate Reconstruction, Lithofacies Paleogeography and Paleoenvironment*. Beijing: Geological Publishing House (in Chinese).

Li, S.T., S.G. Yang, C.L. Wu, J.F. Huang, S.T. Cheng, W.C. Xia, and G.R. Zhao. 1987. Late Mesozoic rifting in Northeast China and Northeast Asia fault basin system. *Scientia Sinica. Series B* 2: 185–195 (in Chinese).

Li, Z.X., D.D. Wang, D.W. Lv, Y. Li, H.Y. Liu, P.L. Wang, Y. Liu, J.Q. Liu, and D.D. Li. 2018. The geologic settings of Chinese coal deposits. *International Geology Review* 60 (5–6): 548–578. https://doi.org/10.1080/00206814.2017.1324327.

Liu, B.P., and Q.Q. Quan. 1996. *Course of Geohistory*. 3rd ed. Beijing: Geological Publishing House (in Chinese).

Liu, G.H. 1990. Permo-Carboniferous paleogeography and coal accumulation and their tectonic control in the north and South China continental plates. *International Journal of Coal Geology* 16 (1): 73–117. https://doi.org/10.1016/0166-5162(90)90014-P.

Liu, G.J., P.Y. Yang, Z.C. Peng, and C.L. Chou. 2004. Petrographic and geochemical contrasts and environmentally significant trace elements in marine-influenced coal seams, Yanzhou mining area, China. *Journal of Asian Earth Sciences* 23 (4): 491–506. https://doi.org/10.1016/j.jseaes.2003.07.003.

Lu, J., L.Y. Shao, L.M. Ran, S.C. Su, K.M. Wei, Y.Z. Sun, J.F. Chen, and X.H. Yu. 2008. A sequence stratigraphic analysis and coal accumulation of Late Triassic coal measures in the Baoding Basin. *Coal Geology and Exploration* 36 (6): 1–6 (in Chinese with English abstract).

Marshall, J.E.A., J. Lakin, I. Troth, and S.M. Wallace-Johnson. 2020. UV-B radiation was the Devonian-Carboniferous boundary terrestrial extinction kill mechanism. *Science Advances* 6 (22): eaba0768. https://doi.org/10.1126/sciadv.aba0768.

Mills, B.J.W., C.M. Belcher, T.M. Lenton, and R.J. Newton. 2016. A modeling case for high atmospheric oxygen concentrations during the Mesozoic and Cenozoic. *Geology* 44 (12): 1023–1026. https://doi.org/10.1130/G38231.1.

Mu-Qiu, C. 1979. Microscopic characteristics of Late Carboniferous coal in China. In *9th International Congress of Carboniferous Stratigraphy and Geology. Washington and Champaign-Urbana*, vol. 4, 555–559.

Petersen, H.I., and S. Lindström. 2012. Synchronous wildfire activity rise and mire deforestation at the Triassic–Jurassic boundary. *PLoS One* 7 (10): e47236. https://doi.org/10.1371/journal.pone.0047236.

Premovic, P.I. 2006. The Late Paleozoic oxygen pulse and accumulations of petroleum source rocks and coal. *Journal of the Serbian Chemical Society* 71 (2): 143–147. https://doi.org/10.2298/JSC0602143P.

Preto, N., E. Kustatscher, and P.B. Wignall. 2010. Triassic climates — State of the art and perspectives. *Palaeogeography, Palaeoclimatology, Palaeoecology* 290 (1-4): 1–10. https://doi.org/10.1016/j.palaeo.2010.03.015.

Qi, M., X.L. Rong, D.Z. Tang, J. Xia, and M. Wolf. 1994. Petrographic and geochemical characterization of pale and dark brown coal from Yunnan province, China. *International Journal of Coal Geology* 25 (1): 65–92.

Qin, J.B., S.F. Wu, X.H. Wang, D.X. Yuan, and H.Y. Yu. 2009. Coal accumulating law and resources prediction of Jurassic coalfield in northern Zhangjiakou. *Acta Geologica Sinica* 83 (5): 738–747 (in Chinese with English abstract).

Querol, X., A. Alastuey, A. Lopez-Soler, F. Plana, R.S. Zeng, J.H. Zhao, and X.G. Zhuang. 1999. Geological controls on the quality of coals from the West Shandong mining district, eastern China. *International Journal of Coal Geology* 42 (1): 63–88. https://doi.org/10.1016/S0166-5162(99)00030-0.

Querol, X., A. Alastuey, X.G. Zhuang, J.C. Hower, A. Lopez-Soler, F. Plana, and R.S. Zeng. 2001. Petrology, mineralogy and geochemistry of the Permian and Triassic coals in the Leping area, Jiangxi Province, Southeast China. *International Journal of Coal Geology* 48 (1): 23–45. https://doi.org/10.1016/S0166-5162(01)00036-2.

Retallack, G.J., J.J. Veevers, and R. Morante. 1996. Global coal gap between Permian–Triassic extinction and Middle Triassic recovery of peat-forming plants. *Geological Society of America Bulletin* 108 (2): 195–207. https://doi.org/10.1130/0016-7606(1996)108<0195:GCGBPT>2.3.CO;2.

Richardson, A.R., C.F. Eble, J.C. Hower, and J.M.K. O'Keefe. 2012. A critical re-examination of the petrology of the no. 5 block coal in eastern Kentucky with special attention to the origin of inertinite macerals in the splint lithotypes. *International Journal of Coal Geology* 98: 41–49. https://doi.org/10.1016/j.coal.2012.04.003.

Rimmer, S.M., S.J. Hawkins, A.C. Scott, and W.L. Cressler. 2015. The rise of fire: Fossil charcoal in Late Devonian marine shales as an indicator of expanding terrestrial ecosystems, fire, and atmospheric change. *American Journal of Science* 315 (8): 713–733. https://doi.org/10.2475/08.2015.01.

Rimmer, S.M., and A.C. Scott. 2006. Charcoal (inertinite) in Late Devonian marine black shales: Implications for terrestrial and marine systems and for paleo-atmospheric composition. European Geosciences Union General Assembly, April 2–7, 2006, Vienna, Austria. *Geophysical Research Abstracts* 8: 07972.

Robinson, J.M. 1989. Phanerozoic O_2 variation, fire, and terrestrial ecology. *Palaeogeography, Palaeoclimatology, Palaeoecology* 75 (3): 223–240. https://doi.org/10.1016/0031-0182(89)90178-8.

Robinson, J.M. 1991. Phanerozoic atmospheric reconstructions: A terrestrial perspective. *Palaeogeography, Palaeoclimatology, Palaeoecology* 97 (1–2): 51–62. https://doi.org/10.1016/0031-0182(91)90181-P.

Royer, D.L., R.A. Berner, I.P. Montañez, N.J. Tabor, and D.J. Beerling. 2004. CO_2 as a primary driver of Phanerozoic climate. *GSA Today* 14 (3): 3–7.

Schobben, M., W.J. Foster, A.R.N. Sleveland, V. Zuchuat, H.H. Svensen, S. Planke, D.P.G. Bond, F. Marcelis, R.J. Newton, P.B. Wignall, and S.W. Poulton. 2020. A nutrient control on marine anoxia during the end-Permian mass extinction. *Nature Geoscience* 13 (9): 640–646. https://doi.org/10.1038/s41561-020-0622-1.

Scotese, C.R. 2002. Paleomap. http://www.scotese.com.

Scott, A.C. 2000. The pre-quaternary history of fire. *Palaeogeography, Palaeoclimatology, Palaeoecology* 164 (1): 281–329. https://doi.org/10.1016/S0031-0182(00)00192-9.

Scott, A.C. 2002. Coal petrology and the origin of coal macerals: A way ahead? *International Journal of Coal Geology* 50 (1): 119–134. https://doi.org/10.1016/S0166-5162(02)00116-7.

Scott, A.C., and I.J. Glasspool. 2006. The diversification of Paleozoic fire systems and fluctuations in atmospheric oxygen concentration. *Proceedings of the National Academy of Sciences of the United States of America* 103 (29): 10861–10865. https://doi.org/10.1073/pnas.0604090103.

Scott, A.C., and I.J. Glasspool. 2007. Observations and experiments on the origin and formation of inertinite group macerals. *International Journal of Coal Geology* 70 (1): 53–66. https://doi.org/10.1016/j.coal.2006.02.009.

Scott, A.C., B.H. Lomax, M.E. Collinson, G.R. Upchurch, and D.J. Beerling. 2000. Fire across the K–T boundary: Initial results from the Sugarite coal, New Mexico, USA. *Palaeogeography, Palaeoclimatology, Palaeoecology* 164 (1-4): 381–395. https://doi.org/10.1016/S0031-0182(00)00182-6.

Sellwood, B.W., and P.J. Valdes. 2008. Jurassic climates. *Proceedings of the Geologists' Association* 119 (1): 5–17. https://doi.org/10.1016/S0016-7878(59)80068-7.

Sen, S., S. Naskar, and S. Das. 2016. Discussion on the concepts in paleoenvironmental reconstruction from coal macerals and petrographic indices. *Marine and Petroleum Geology* 73: 371–391. https://doi.org/10.1016/j.marpetgeo.2016.03.015.

Shao, K., L.Y. Shao, Y.L. Qu, Q. Zhang, J. Wang, D. Gao, D.D. Wang, and Z. Li. 2013. Study of sequence stratigraphy of the Early cretaceous coal measures in northeastern China. *Journal of China Coal Society* 38 (Supp. 2): 423–433 (in Chinese with English abstract).

Shao, L.Y., D. Gao, Z. Luo, and P.F. Zhang. 2009. Sequence stratigraphy and palaeogeography of the Lower and Middle Jurassic coal measures in Turpan–Hami Basin. *Journal of Palaeogeography (Chinese Edition)* 11 (2): 215–224 (in Chinese with English abstract).

Shao, L.Y., T. Jones, R. Gayer, S.F. Dai, S.S. Li, Y.F. Jiang, and P.F. Zhang. 2003. Petrology and geochemistry of the high-Sulphur coals from the Upper Permian carbonate coal measures in the Heshan coalfield, southern China. *International Journal of Coal Geology* 55 (1): 1–26. https://doi.org/10.1016/S0166-5162(03)00031-4.

Shao, L.Y., Y.J. Li, F.X. Jin, C.X. Gao, C. Zhang, W.L. Liang, G.M. Li, Z.S. Chen, Z. Q. Peng, and A.G. Cheng. 2014. Sequence stratigraphy and lithofacies palaeogeography of the Late Triassic coal measures in South China. *Journal of Palaeogeography (Chinese Edition)* 16 (5): 613–630 (in Chinese with English abstract).

Shao, L.Y., X.T. Wang, J. Lu, D.D. Wang, and H.H. Hou. 2017. A reappraisal on development and prospect of coal sedimentology in China. *Acta Sedimentologica Sinica* 35 (5): 1016–1031 (in Chinese with English abstract).

Shaviv, N.J., and J. Veizer. 2003. Celestial driver of Phanerozoic climate? *GSA Today* 13 (7): 4–10. https://doi.org/10.1130/1052-5173(2003)013<0004:CDOPC>2.0.CO;2.

Shi, H.N., F.Y. Meng, and J.J. Tian. 2011. Coal-forming environment and sedimentary characteristics of Badaowan Formation in Yili Basin. *Journal of Xi'an University of Science and Technology* 31 (1): 33–38 (in Chinese with English abstract).

Silva, M.B., and W. Kalkreuth. 2005. Petrological and geochemical characterization of Candiota coal seams, Brazil — Implication for coal facies interpretations and coal rank. *International Journal of Coal Geology* 64 (3–4): 217–238. https://doi.org/10.1016/j.coal.2005.04.003.

Silva, M.B., W. Kalkreuth, and M. Holz. 2008. Coal petrology of coal seams from the Leão-Butiá coalfield, Lower Permian of the Paraná Basin, Brazil — Implications for coal facies interpretations. *International Journal of Coal Geology* 73 (3): 331–358. https://doi.org/10.1016/j.coal.2007.08.002.

Snyman, C.P. 1961. A comparison between the petrography of south African and some other Palaeozoic coals. *Nuwe Reeks* 15: 33.

Spicer, R.A. 2003. Changing climate and biota. In *The Cetaceous World*, ed. P. Skelton, 85–163. Cambridge: Cambridge University Press.

Stach, E. 1990. *Stach's Textbook of Coal Petrology*, 3rd ed. Beijing: China Coal Industry Publishing House (in Chinese).

Sun, S.L. 2013. *National Coal Resources Potential Evaluation*. Beijing: China Coal Geology Administration (in Chinese).

Sun, Y.Z., W. Püttmann, W. Kalkreuth, and B. Horsfield. 2002. Petrologic and geochemical characteristics of seam 9-3 and seam 2, Xingtai coalfield, northern China. *International Journal of Coal Geology* 49 (4): 251–262. https://doi.org/10.1016/S0166-5162(01)00067-2.

Tabor, N.J., and C.J. Poulsen. 2008. Palaeoclimate across the Late Pennsylvanian–Early Permian tropical palaeolatitudes: A review of climate indicators, their distribution, and relation to palaeophysiographic climate factors. *Palaeogeography, Palaeoclimatology, Palaeoecology* 268 (3–4): 293–310. https://doi.org/10.1016/j.palaeo.2008.03.052.

Tan, C. 2017. *Sedimentary Characteristics and Paleoclimatic Evolution of the Upper Permian–Middle Upper Triassic Series in the Ordos Basin [PhD Thesis]*. Beijing: China University of Geosciences (Beijing) (in Chinese).

Taylor, G.H., S.Y. Liu, and C.F.K. Diessel. 1989. The cold-climate origin of inertinite-rich Gondwana coals. *International Journal of Coal Geology* 11 (1): 1–22. https://doi.org/10.1016/0166-5162(89)90110-9.

Taylor, G.H., M. Teichmüller, A. Davis, C.F.K. Diessel, R. Littke, and P. Robert. 1998. *Organic petrology*, 10–205. Berlin: Gebruder Borntraeger.

Teichmüller, M. 1952. *Vergleichende mikroskopische Untersuchungen versteinerter Torfie des Ruhrkarbons und der daraus entstanden Steinkohlen*, 607–613. Heerlen: 3rd Carboniferous Congress.

Teichmüller, M. 1989. The genesis of coal from the viewpoint of coal petrology. *International Journal of Coal Geology* 12 (1): 1–87. https://doi.org/10.1016/0166-5162(89)90047-5.

Tian, Y., Z.X. Li, L.Y. Shao, D.D. Wang, and M.P. Li. 2011. Upper Triassic Series Wayaobu Formation sequence stratigraphic and coal accumulation characteristic studies in Ordos Basin. *Coal Geology of China* 23 (8): 13–17 27 (in Chinese with English abstract).

Vail, P.R., R.M. Mitchum Jr., and S. Thompson III. 1977. Seismic stratigraphy and global changes of sea level, part 4: Global cycles of relative changes of sea level. In *Seismic Stratigraphy: Applications to Hydrocarbon Exploration. AAPG Memoir*, vol. 26, ed. C.E. Payton, 83–97.

Van Niekerk, D., G.D. Mitchell, and J.P. Mathews. 2010. Petrographic and reflectance analysis of solvent-swelled and solvent-extracted south African vitrinite-rich and inertinite-rich coals. *International Journal of Coal Geology* 81 (1): 45–52. https://doi.org/10.1016/j.coal.2009.10.021.

Virgili, C. 2008. The Permian–Triassic transition: Historical review of the most important ecological crises with special emphasis on the Iberian Peninsula and Western-Central Europe. *Journal of Iberian Geology* 34 (1): 123–158.

Wang, D.D., Q. Mao, G.Q. Dong, S.P. Yang, D.W. Lv, and L.S. Yin. 2019. The genetic mechanism of inertinite in the Middle Jurassic inertinite-rich coal seams of the southern Ordos Basin. *Journal of Geological Research* 1 (3): 1–15.

Wang, J. 2002. *Experimental Study on the Influence of Coal Quality (Species) Characteristics on Power Plant Boilers [Master Thesis]*. Hangzhou: Zhejiang University (in Chinese).

Wang, Y., L.Q. Li, and X.Q. Zhang. 2016. Inertinite of coal-rocks and its application to the paleoenvironment reconstruction of peat and mire. *Geological Review* 62 (2): 375–380 (in Chinese with English abstract).

Ward, P., C. Labandeira, M. Laurin, and R.A. Berner. 2006. Confirmation of Romer's gap as a low oxygen interval constraining the timing of initial arthropod and vertebrate terrestrialization. *Proceedings of the National Academy of Sciences of the United States of America* 103 (45): 16818–16822. https://doi.org/10.1073/pnas.0607824103.

Wildman, R.A., L.J. Hickey, M.B. Dickinson, R.A. Berner, J.M. Robinson, M. Dietrich, R.H. Essenhigh, and C.B. Wildman. 2004. Burning of forest materials under Late Paleozoic high atmospheric oxygen levels. *Geology* 32 (5): 457–460. https://doi.org/10.1130/G20255.1.

Wollenweber, J., J. Schwarzbauer, R. Littke, H. Wilkes, A. Armstroff, and B. Horsfield. 2006. Characterisation of non-extractable macromolecular organic matter in Palaeozoic coals. *Palaeogeography, Palaeoclimatology, Palaeoecology* 240 (1–2): 275–304. https://doi.org/10.1016/j.palaeo.2006.03.053.

Wu, K.P., Y.X. Liu, B.Z. Ji, and Y.P. Lu. 2008. Sedimentary coal-accumulating environment and prospecting coal prospect of Meihe Basin. *Jilin Geology* 27 (3): 24–29 33 (in Chinese with English abstract).

Xiao, X.M., B.Q. Zhao, Z.L. Thu, Z.G. Song, and R.W.T. Wilkins. 2005. Upper Paleozoic petroleum system, Ordos Basin, China. *Marine and Petroleum Geology* 22 (8): 945–963. https://doi.org/10.1016/j.marpetgeo.2005.04.001.

Yan, Z.M., L.Y. Shao, I.J. Glasspool, J. Wang, X.T. Wang, and H. Wang. 2019. Frequent and intense fires in the final coals of the Paleozoic indicate elevated atmospheric oxygen levels at the onset of the end-Permian mass extinction event. *International Journal of Coal Geology* 207: 75–83. https://doi.org/10.1016/j.coal.2019.03.016.

Yang, Y.K. 1996. *Atlas for Coal Petrography of China*. Xuzhou: China University of Mining and Technology Press (in Chinese).

Zhang, G.C., Z.X. Li, Y.P. He, H.H. Zhang, L. Jing, H.L. Shen, and N. Fu. 2010. Coal geochemistry of Qiongdongnan Basin. *Natural Gas Geoscience* 21 (5): 693–699 (in Chinese with English abstract).

Zhang, Q., and J.J. Wu. 1996. Trend of correlation between macerals and palynological types in coal in Huanglong coalfield. *Coal Geology and Exploration* 24 (1): 15–19 (in Chinese).

Zhang, T. 1995. *Depositional Environment and Coal-Accumulating Regularities of Main Coal-Accumulating Stages of China*. Beijing: Geological Publishing House (in Chinese with English table of contents and abstract).

Zhang, Z.H., C.S. Wang, D.W. Lv, W.W. Hay, T.T. Wang, and S. Cao. 2020. Precession-scale climate forcing of peatland wildfires during the early Middle Jurassic greenhouse period. *Global and Planetary Change* 184: 103051. https://doi.org/10.1016/j.gloplacha.2019.103051.

Zhao, X.D., D.R. Zheng, G.W. Xie, H.C. Jenkyns, C.G. Guan, Y.N. Fang, J. He, X.Q. Yuan, N.H. Xue, H. Wang, S. Li, E.A. Jarzembowski, H.C. Zhang, and B. Wang.

2020. Recovery of lacustrine ecosystems after the end-Permian mass extinction. *Geology* 48 (6): 609–613. https://doi.org/10.1130/G47502.1.

Zhao, Y., B. Chen, S.H. Zhang, J.M. Liu, J.M. Hu, J. Liu, and J.L. Pei. 2010. Pre-Yanshanian geological events in the northern margin of the North China Craton and its adjacent areas. *Geology in China* 37 (4): 900–915 (in Chinese with English abstract).

Zhao, Y.N., D.N. Wang, and X.Y. Sun. 1995. Early Tertiary palynoflora: Its relation to Paleoclimate, paleogeography and paleoecology of China. *Professional Papers of Stratigraphy and Palaeontology* 26 (2): 115–123 (in Chinese with English abstract).

Zheng, Z.H. 2008. Early Carboniferous sedimentary environments and coal forming characteristics of Guangxi Province, China. *Nanfang Guotu Ziyuan* (1): 39–40 (in Chinese).

Zhou, H.T., Z.M. Fu, Z. Li, Q. Zeng, S.Q. Du, and Z.J. Song. 1990. Depositional environments and coal-forming sedimentary characteristics of Taiyuan Formation of Late Carboniferous in Pingdingshan coal-field, Henan Province. *Acta Sedimentologica Sinica* 8 (3): 35–45 (in Chinese with English abstract).

Zhuang, X.G., X. Querol, A. Alastuey, F. Plana, N. Moreno, J.M. Andrés, and J. L. Wang. 2007. Mineralogy and geochemistry of the coals from the Chongqing and Southeast Hubei coal mining districts, South China. *International Journal of Coal Geology* 71 (2): 263–275. https://doi.org/10.1016/j.coal.2006.09.005.

Publisher's Note